HBFF-SVD Force Field Treatment of Ni(II) Porphine: Important Long Range Cross Terms

Hui-Hsu (Gavin) Tsai and M. Cather Simpson*

Department of Chemistry, Case Western Reserve University, Cleveland, Ohio 44106

Received: August 2, 2002

A systematic exploration of the importance of cross terms in the Ni(II) porphine force field is reported. Several force fields of varying complexity were generated using a modification of the Hessian-biased singular value decomposition (HBFF-SVD) approach originally developed by Goddard et al. The X-ray crystal structure, a B3LYP/6-31G(d,p) Hessian matrix, and experimental vibrational frequencies were used. The diagonal-only force field is inadequate for reproducing experimental frequencies. As anticipated, inclusion of 1,2 and 1,3 cross terms significantly improves results (total rms error 14.6 cm^{-1}; in-plane rms error = 12.0 cm^{-1}). The longer range terms in a complete, in-plane, force field improve performance dramatically (in-plane rms error = 4.8 cm^{-1}). A total of 83 long range interaction constants have values ≥10 kcal/(mol geom-unit), and 5 are greater than 20 kcal/(mol geom-unit). For example, 1,6- and 1,9-($C_\alpha-C_m$)−($C_\alpha-C_m$) stretch−stretch, 1,4-($C_\alpha-N$)−($C_\alpha-C_m$), and 1,4-($C_\beta-C_\beta$)−($C_\alpha-N-C_\alpha$) stretch−bend interactions are large and positive. Coupling in- and out-of-plane motions (TORX) enhances out-of-plane accuracy. Though isotopomer data were omitted from the optimization, the HBFF-SVD force fields reproduce these data with high fidelity. Finally, the HBFF-SVD force fields are compared in detail to previous normal-mode analysis and scaled quantum mechanics studies of Ni porphine.

I. Introduction

Metalloporphyrins have provided chemists a rich area of study for decades. Their biological and technological importance has spurred the detailed examination of their static and dynamic structural and spectral behavior (e.g., see ref 1). In addition, their high symmetry, large optical cross-sections, and significant vibronic character make this class of molecules intrinsically intriguing. The vibrational spectroscopy of porphyrins has been an area of particularly intense research focus.[2,3] The infrared and resonance Raman spectra are very well characterized for many porphyrins and porphyrin-containing systems. Drawing the correlations between the observed vibrational features and the molecular structure is a challenging aspect of this research.

Considerable effort has been expended in theoretical studies of porphyrins toward this goal, and a great deal of progress has been made (for a recent review, see ref 4). Quantum mechanical methods (for recent reviews, see refs 5 and 6), classical force field analyses,[7−13] and combinations of the two[14−18] have been employed. Particular attention has been paid to nickel porphyrins, making this class of metalloporphyrins a "standard." The sensitivity of the Ni porphyrin planarity to peripheral substitution, and the possible biological implications thereof, have maintained a high level of interest in these molecules (for recent reviews, see refs 19−21). The extensive and detailed structural and vibrational literature available for Ni porphyrins with a variety of peripheral substituents provides invaluable guidance for theoretical studies.

Normal-mode analysis (NMA) has been particularly fruitful for studying the vibrational structure of a wide range of molecules.[22] In particular, this empirical force field method has been used with great success to determine normal coordinates, force constants, and vibrational assignments for several porphyrins and their isotopomers. In a now classic study, Kitagawa and co-workers first applied NMA to Ni(II) octaethyl porphyrin (NiOEP) in 1978.[7,9] Spiro and co-workers have since developed a consistent force field for the porphyrin macrocycle.[10−12] This NMA-based force field has recently been optimized further.[13,18,23]

Although NMA has proven quite useful for evaluating metalloporphyrin vibrations, the method has some well-known limitations. First, NMA is inherently underdetermined, and the resulting force field is not unique. Even with isotope substitution data, there are more parameters in the force field than there are data points to which to fit them, a problem that increases in severity with the molecule size. This difficulty is related to another drawback. To limit the number of adjustable parameters, the user chooses a subset of possible force field terms. Arbitrariness is thereby introduced, particularly in the off-diagonal portion of the force field. In particular, longer range cross terms are often neglected, though they may be quite significant. These choices can influence the outcome substantially and in ways difficult to predict because of the entangled influences force field terms have upon one another.

A new variation on NMA has recently been developed by Unger et al.[24,25] The molecule is described by independent, local, symmetry units, each consisting of a central atom and its bonded neighbors. This approach allows for easy transferability and reduces the number of adjustable parameters. Accuracy can be further refined, unfortunately at the expense of objectivity, by allowing user-selected interactions among symmetry groups. The approach appears to be a promising alternative to traditional NMA, though the number of molecules treated thus far is relatively limited. Though the accuracy of calculated frequencies does not appear to be improved over NMA, the reduction in the number of parameters is quite significant. Treatment of porphyrins, including Ni porphine, yielded results on par with earlier NMA studies.

* To whom correspondence should be addressed. E-mail: mcs9@po.cwru.edu. Phone: (216) 368-1911. Fax: (216) 368-3006.

10.1021/jp0218037 CCC: $25.00
Published on Web 01/04/2003

One way to avoid the difficulties of NMA and yet address the same spectrum-structure issues uses quantum mechanics (QM) to directly evaluate structures, frequencies, and intensities. With an adequate basis set, both Hartree−Fock (HF)-based and gradient-corrected density functional theory (DFT) methods calculate these quantities with fair accuracy.[26,27] Errors usually originate from inadequate treatment of electron correlation and from comparison of harmonic calculated frequencies with anharmonic experimental ones. Because these types of errors are systematic, simple scaling of the frequencies can greatly improve accuracy.[28,29] However, despite the tremendous advances in quantum mechanical methods and programs, accurate calculations on larger molecules are still too slow and require too much memory to perform routinely.

QM can be used to generate a force field of classical form, thereby merging objectivity and accuracy with cost efficiency and speed. This hybrid approach has been used widely to study a range of molecules (see references in ref 30, for example) including porphyrins.[14−18,23] Pulay et al. have developed an approach that involves performing a fairly high-level QM calculation, either using nonredundant "natural" coordinates or transforming the result into those coordinates, then empirically scaling the resultant force constants to fit experimental frequencies.[31−34] Scaling can be done individually or in groups of related coordinates.[34] Where available, isotope shifts further optimize the scaling. This scaled quantum mechanics (SQM) has been used to derive a set of eleven transferable scaling factors for organic molecules, with very good performance.[33] The rms deviation of ∼300 modes in a set of medium-sized organic molecules was only 12.6 cm^{-1}.

SQM has been applied to a handful of porphyrins[14−18] including Ni porphine[18] using quantum mechanics at the B3LYP/6-31G(d)/VTZ(Ni) level, a set of nonredundant natural internal coordinates, and scaling factors derived by optimization of a previously obtained transferable set with H_2-porphine natural abundance and isotopomer spectra.[16] Frequencies and IR and nonresonance Raman intensities for H_2-porphine were predicted well, and SQM treatment of Ni porphine was clearly superior to even the newly optimized NMA force field.

Advantages of SQM over NMA include increased accuracy and improved objectivity. Unless one chooses to individually scale all terms, the number of adjustable parameters is greatly reduced. Some arbitrariness remains, as grouping of scaling factors is done manually on the basis of chemical intuition, and the details of grouping can significantly affect the outcome.[33,34] SQM suffers from a few other drawbacks as well. Though scaling the force constants is physically more satisfying than scaling the frequencies, SQM still involves empirical scaling factors. The recommended nonredundant natural coordinates are not particularly convenient for those who wish to use the force field for calculating structures, frequencies and classical dynamics of new molecules. Readily available programs typically use highly redundant internal coordinates, necessitating a transformation that Pulay et al. indicate few know how to do. Finally, neither the SQM nor the NMA methods include nonbonding interactions. These forces are particularly important in large molecules, where regions of the molecule distant in terms of bond connectivity may interact through space via electrostatic, hydrogen bonding, or van der Waals forces. Nonbonding interactions are also considerably important in biological systems, where the protein-active site (e.g., porphyrin) interactions can have significant functional consequences.

A method that overcomes many of these difficulties has been developed by Goddard and co-workers[35−37] and applied here to Ni(II) porphine (NiP) (Figure 1). Like SQM, this approach uses QM to obtain an accurate, experimentally corrected force field. However, Goddard et al.'s method differs from SQM in some important ways. SQM uses QM and nonredundant internal coordinates to reduce the number of adjustable parameters in the force field. The approach Goddard et al. take is to use QM to increase the number of data points to which to fit a highly redundant force field. A large number of adjustable parameters (force constants, equilibrium geometry variables, nonbonding variables) is retained; the geometry (experimental or calculated) and the elements of an experimentally transformed QM Hessian (second derivative of the energy with respect to coordinates) matrix are treated as data to which to fit the force field. Thus, instead of the $3N - 6$ frequency and $3N - 6$ force (geometry) constraints, there are $(3N - 3)(3N - 6)/2$ unique "data" points for the fitting procedure. Except in a few special cases, this Hessian-biased force field (HBFF) method is over- rather than under-determined. Though not done in this study, the fit can be improved by including other experimental data (e.g., isotope shifts, polarizability, crystal properties) and by fitting directly to the frequencies as a final refinement. Singular-value decomposition (SVD) can identify necessary and unnecessary force field terms. In principle, then, HBFF-SVD can generate an experimentally corrected, QM-guided force field without empirical scaling factors and user-made choices regarding the inclusion of diagonal and off-diagonal force constant terms. This method has been used to treat small and medium sized organic molecules, polymers, and several inorganic systems with good results.[38−43]

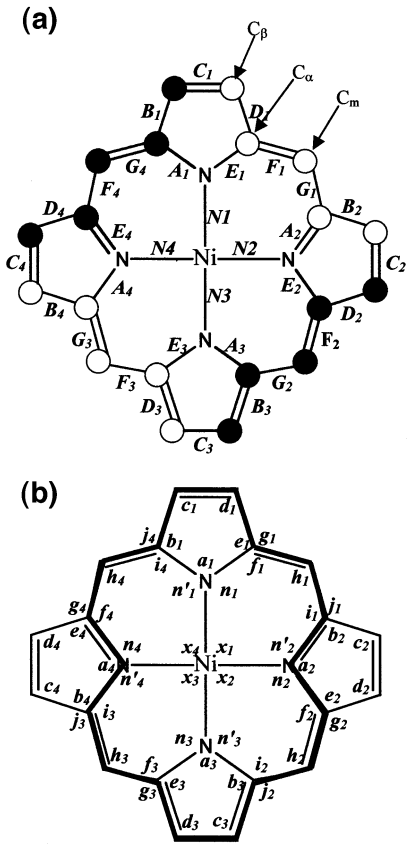

Figure 1. Nickel porphine. (a) Atom and bond labels are shown. The out-of-plane b_{1u} ruffling distortion coordinate is also depicted; atoms that move above and below the macrocycle plane are marked with open and closed circles, respectively. (b) Angle labels are shown. The conjugation pathway for this resonance structure is marked with a black outline.

Here we report the application of HBFF-SVD to the calculation of an accurate classical force field of Ni(II) porphine (NiP) (Figure 1). We performed this detailed study for several reasons beyond the significance of this class of molecules in biology, technology, and basic science. Although this system has previously been investigated, no systematic examination of cross terms has been reported, to our knowledge. In particular, a complete exploration of all binary, long range, stretch−stretch, stretch−bend, and bend−bend cross terms would lend considerable insight into the structure-spectrum relationship. The highly symmetric, conjugated nature of the porphyrin macrocycle makes the importance of these long range interactions particularly likely. In addition, the structural, spectral, and functional consequences of porphyrin nonplanarity can be quite significant. For this reason, we explored the coupling of in-plane and out-of-plane degrees of freedom. van der Waals interactions were included as well. More minor motivations include the stringent test this system provides for the HBFF-SVD method. We evaluated the ability of HBFF-SVD to faithfully represent the potential energy surface near the minimum for this large molecule in (very) redundant internal coordinates.

The crystal structure of NiP[44] and recent, very careful, vibrational assignments by Kozlowski et al.[18] were used, and the quantum mechanical Hessian matrix was generated by using the hybrid density functional B3LYP and a moderate Gaussian basis set (6-31G(d,p)). Several important modifications were made to the fitting method to improve speed and accuracy. Force fields were created at several levels of complexity, adding classes of cross terms systematically. Force field accuracy was assessed by the ability to reproduce experimental frequencies of natural abundance and isotopically substituted NiP. The isotope information is an important, independent test of force field quality, as these data are not used in the optimization procedure.

The HBFF-SVD method performed significantly better than NMA, and on par with SQM. As expected, the force field with only diagonal terms was inadequate for reproducing vibrational frequencies. Most force fields employ short range cross terms, and the inclusion of these improved the HBFF-SVD NiP force field significantly. Further accuracy was obtained by adding long range, in-plane cross terms, but no improvement was gained by coupling in-plane and out-of-plane degrees of freedom. New, previously undiscovered, long range cross terms were found to be quite significant in faithfully reproducing vibrational frequencies and in providing insight into the structure-spectrum relationship in this important class of molecules. In short, the performance of the HBFF-SVD procedure on this challenging problem was excellent.

II. Computational Methods

HBFF-SVD was employed to generate a set of classical force fields for NiP. This approach[35−37] has been substantially improved and extended by us to study larger systems, particularly those with conjugation. As the method has been described fully elsewhere,[35−37] we detail only the particulars of the NiP study and our improvements.

Briefly, the algorithm is as follows. DFT calculated a Hessian matrix, $\mathbf{H}^{QM}$, with elements $(\partial^2 E/\partial q_i \partial q_j)_0$. This matrix was corrected by the observed fundamental frequencies to form $\mathbf{H}^{expt}$, and then a chosen classical force field was fit to it and to the experimental geometry. A wide range in force field complexity was studied. To assess the quality of the method and to probe the effects of various cross terms, each force field's ability to reproduce vibrational frequencies of natural abundance NiP and isotope shifts was examined.

TABLE 1: Experimental and Calculated Geometry of Ni Porphine

	expt[a]	BLYP/6-31G(d,p)[c]	B3LYP/6-31G(d,p)[c]	B3LYP/6-31G(d),VTZ(Ni)[b]
		Bond Lengths (Å)		
Ni−N	1.951(2)	1.9394	1.9425	1.9659
C_α−N	1.379(2)	1.3960	1.3794	1.3778
C_α−C_β	1.435(4)	1.4467	1.4389	1.4400
C_α−C_m	1.371(3)	1.3901	1.3815	1.3823
C_β−C_β	1.347(3)	1.3700	1.3585	1.3587
rms error		*0.0168*	*0.0078*	*0.0099*
		Bond Angles (deg)		
N−Ni−N	90.0(1)	90.00	90.00	90.00
Ni−N−C_α	127.8(2)	127.76	127.73	127.66
C_α −N−C_α	104.3(2)	104.47	104.54	104.68
N− C_α−C_β	111.0(3)	110.93	111.10	111.06
N− C_α−C_m	125.4(3)	124.70	125.02	125.35
C_m−C_α−C_β	123.6(2)	124.06	123.69	123.55
C_α−C_β−C_β	106.8(2)	106.80	106.61	106.60
C_α−C_m−C_α	123.5(2)	122.73	123.02	123.58
rms error		*0.42*	*0.26*	*0.17*
		Ruffling Angle (deg)		
C_α−N- - -N−C_α	1.7	28.8	22.8	11.8

[a] The experimental geometry is from ref 44. [b] The B3LYP/6-31G(d),VTZ(Ni) results are from ref 18. [c] The BLYP/6-31G(d,p) and B3LYP/6-31G(d,p) results are from this study.

Geometry and Hessian. All geometry optimizations and harmonic frequency calculations were performed on a PC platform using the Gaussian 98 suite of programs.[45] Symmetry was used where appropriate, and all calculated frequencies were real. The BLYP (Becke's gradient-corrected exchange[46] and the Lee−Yang−Parr gradient-corrected correlation[47] functionals) and B3LYP (Becke's three-parameter exchange functional[48] and the Lee−Yang−Parr gradient-corrected correlation functional[47]) density functionals were employed, as indicated. All reported calculations used the moderate-sized 6-31G(d,p)[49] basis set for all atoms, including Ni. All Hessians fit by HBFF-SVD were computed at the B3LYP/6-31G(d,p) level.

Force fields were fit using the experimental NiP geometry determined by X-ray crystallography (Table 1).[44] Examination of the cross-macrocycle C_α−N- -N−C_α dihedral shows a slightly nonplanar conformation in the crystal. The distortion is of the ruffling (b_{1u}) type, with opposite pyrrole rings twisted in opposite directions relative to the macrocycle plane (Figure 1).

The alternative choice would be to use a quantum mechanical geometry. Hartree−Fock (HF) self-consistent field theory tends to underestimate bond lengths significantly.[26] For porphyrins, HF has the added disadvantage that the stationary geometry is grossly incorrect, with alternating bond lengths.[6,50] Electron correlation (e.g., MP2) corrects this problem but is prohibitively expensive for molecules the size of porphyrins. DFT includes electron correlation more efficiently and generally calculates geometries accurately, particularly for molecules consisting of first row elements. Hybrid functionals such as B3LYP (gradient corrected correlation + some exact HF exchange) exhibit excellent accuracy, with average bond length errors of 0.003−0.011 Å, though this appears to result from error cancellation; HF tends to underestimate bond lengths, whereas gradient-corrected DFT tends to overestimate.[26,27] DFT generally yields absolute errors of less than ∼2°, with hybrid functional mean absolute errors <1°.[27] Dihedral angles are important determinants of overall geometry as well. A study of conjugated molecules shows that DFT generally produces geometries that are more planar than do HF-based methods.[51]

DFT calculations of the NiP geometry have been performed by us and others (Table 1),[5,6,18] and comparison to the crystal

structure shows the general trends discussed above. The only significant differences between the experimental and DFT geometries are the ruffling angle (τ_{ruf} = C$_\alpha$−N- -N−C$_\alpha$ dihedral) and the Ni−N bond length. These two degrees of freedom are related. Ruffling (Figure 1) allows the Ni−N bond to shorten to a more energetically favored value,[52] but at the expense of conjugation. Because of this interplay, the potential energy surface for NiP along the τ_{ruf} coordinate is very flat. The balance point occurs at a slightly different place on the potential energy surface than it does in the crystal. This difference could be due to either the effects of crystal packing or poor performance of DFT in accurately portraying this challenging, flat part of the potential. As we found no compelling reason to prefer the computational findings to the experimental, we decided to use the X-ray results as the most accurate geometry.

The quality of the force field is limited by the quality of the Hessian matrix (elements defined $H_{ij} = (\partial^2 E/\partial q_i \partial q_j)_0$) to which it is fit. Diagonalization of this matrix yields normal mode eigenvectors and harmonic vibrational frequencies. Unfortunately, we do not have access to the "true" Hessian. We therefore generated a quantum mechanical Hessian ($\mathbf{H}^{QM}$) using the B3LYP functional and the 6-31G(d,p) basis set. B3LYP was chosen because, as discussed above, the geometry it predicts is closest to the experimental (Table 1). Also, it reproduces experimental vibrational frequencies with a relatively small, systematic rms error (30.95 cm^{-1}; most values overestimated) (Figure 2). The BLYP functional actually comes closer to the experimental values (rms error = 13.79 cm^{-1}; deviation spread fairly evenly about the mean; not shown). Nonetheless, SQM studies have indicated that, once corrected for systematic errors, the B3LYP harmonic potential is superior;[18] our experience concurs with this finding.

Even high-level ab initio and DFT calculations do not reproduce experimental frequencies exactly. Errors arise from basis set truncation, incomplete treatment of electron correlation, the harmonic approximation, and the influence of the experimental conditions (e.g., solution, solid state). To improve the accuracy of the classical force field, HBFF-SVD systematically corrects $\mathbf{H}^{QM}$ with the experimental frequencies. A back-transformation using the experimental frequencies as the diagonal eigenvalue matrix (λ^{expt}) and the QM normal mode eigenvectors (**N**) generates the experimentally corrected Hessian matrix ($\mathbf{H}^{expt}$):

$$\mathbf{(N)H}^{QM}\mathbf{(N^{-1})} = \lambda^{QM} \tag{1a}$$

$$\mathbf{(N^{-1})}\lambda^{expt}\mathbf{(N)} = \mathbf{H}^{expt} \tag{1b}$$

The force fields were then fit to $\mathbf{H}^{expt}$.

Mismatching experimental and calculated frequencies is a source of potentially large error. The assignments of NiP have recently been revisited by Kozlowski et al.,[18] and were followed here. Where experimental frequencies are missing, SQM results were used. Experimental and SQM frequencies appear in Table 2, for comparison with HBFF-SVD results.

Classical Force Fields. The next step is to choose a classical force field form to which to fit $\mathbf{H}^{expt}$ and the experimental geometry. The general form of the total classical potential energy can be expressed as a sum of a subset of diagonal terms, standard cross terms, nonstandard cross terms, torsional cross terms, and nonbonding interactions, depending upon the level of approximation employed:

$$E^{total} = E^{diag} + E^{stdx} + E^{nstdx} + E^{torx} + E^{nb} \tag{2}$$

The functional forms for all of these types of terms are shown in Table 3.

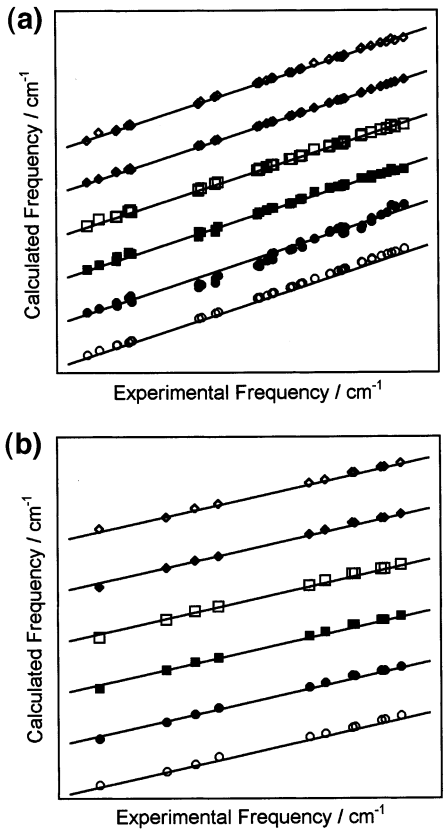

Figure 2. Comparison of experimental and calculated frequencies. Experimental vibrational frequencies of naturally abundant NiP are compared to results from density functional theory at the B3LYP/6-31G(d,p) level (open circles) and from HBFF-SVD force fields: DIAG (filled circles), STDX (filled squares), NSTDX (open squares), CIPX (filled diamonds), and TORX (open diamonds). The comparisons are displaced vertically for displaying. Lines indicate the ideal (experimental value = calculated frequency) situation. The experimental frequencies are from ref 18. (a) In-plane degrees of freedom. (b) Out-of-plane degrees of freedom.

Diagonal Force Field Terms. The diagonal energy terms (E^{diag}) are the traditional bond-stretching, angle-bending, and torsion (Table 3).

Cross (Off-Diagonal) Force Field Terms. Calculated vibrational spectra are quite sensitive to the number and type of cross terms included in the force field. In the "true" force field, many cross terms will have nonzero values. In conjugated molecules such as NiP, some of these important cross terms may be fairly long range in nature. Including all of the possible cross terms, however, is usually prohibited due to the size of the molecule. To address this problem, a systematic approach for including additional cross terms in the force field is needed.

The most basic class of cross terms has been named *standard* (E^{stdx}). This group incorporates 1,2 stretch−stretch (I−J-K: bond I−J with bond J−K), 1,2 stretch−bend (I−J-K: bond I−J with angle I−J-K), and 1,2 bend−bend (two angles sharing two atoms) interactions. The next level of complexity includes *nonstandard* cross terms (E^{nstdx}). E^{nstdx} includes 1,3 stretch−stretch (I−J-K−L: bond I−J with bond K−L), 1,3 bend−bend (I−J-K−L-M: angle I−J-K with angle K−L-M), and 1,3 stretch−bend (I−J-K−L: bond I−J with angle J−K-L) interactions. Longer range stretch−stretch, bend−bend, and stretch−bend couplings have the same form. The *torsion* cross terms (E^{torx}) explore the effect of coupling in-plane and out-of-plane motions through torsion−stretch and torsion−bend interactions (I−J-K−L torsion and the bonds and angles within). Table 3 contains the forms for all of these cross terms.

TABLE 2: Experimental and Calculated Vibrational Frequencies of NiP

	mode	expt[a]	B3LYP/6-31G(d,p)[b]	NMA[c]	SQM[c]	DIAG	STDX	NSTDX	CIPX	TORX
					In-Plane					
A_{1g}										
ν_5	$\nu(C_\beta H)_{sym}$		3261	3097	3100	3114	3113	3110	3110	3110
ν_1	$\nu(C_mH)$		3212	3041	3073	3080	3073	3073	3073	3073
ν_2	$\nu(C_\beta C_\beta)$	1574	1627	1578	1585	1600	1555	1564	1573	1563
ν_3	$\nu(C_\alpha C_m)_{sym}$	1459	1514	1456	1469	1377	1478	1466	1459	1467
ν_4	ν(Pyr half-ring)$_{sym}$	1376	1416	1374	1384	1311	1380	1355	1376	1354
ν_9	$\delta(C_\beta H)_{sym}$	1066	1098	1059	1067	1040	1063	1065	1066	1065
ν_6	ν(Pyr breathing)	995	1026	1003	998	871	975	993	998	994
ν_7	δ(Pyr def)$_{sym}$	732	745	737	732	578	674	710	732	709
ν_8	ν(NiN)	369	382	384	362	323	401	353	373	355
B_{1g}										
ν_{14}	$\nu(C_\beta H)_{sym}$		3261	3097	3100	3114	3113	3110	3110	3110
ν_{10}	$\nu(C_\alpha C_m)_{asym}$	1650	1701	1659	1659	1714	1610	1621	1651	1621
ν_{11}	$\nu(C_\beta C_\beta)$	1505	1564	1510	1521	1523	1516	1507	1505	1508
ν_{12}	ν(Pyr half-ring)$_{sym}$	1383	1426	1324	1394	1321	1379	1382	1381	1383
ν_{13}	$\delta(C_mH)$	1185	1222	1200	1193	1197	1186	1186	1184	1187
ν_{17}	$\delta(C_\beta H)_{sym}$	1058	1092	1060	1062	1039	1064	1061	1062	1062
ν_{15}	ν(Pyr breathing)	1003	1029	1022	999	859	1011	999	1000	997
ν_{16}	δ(Pyr def)$_{sym}$	732	746	728	740	622	741	726	736	722
ν_{18}	ν(NiN)	237	241	254	233	231	217	222	233	210
A_{2g}										
ν_{23}	$\nu(C_\beta H)_{asym}$		3241	3095	3101	3109	3098	3101	3101	3101
ν_{19}	$\nu(C_\alpha C_m)_{asym}$	1611	1659	1616	1615	1682	1581	1585	1611	1584
ν_{20}	ν(Pyr quarter-ring)	1354	1396	1345	1356	1380	1362	1355	1356	1356
ν_{26}	$\delta(C_\beta H)_{asym}$	1317	1356	1303	1329	1327	1336	1316	1318	1316
ν_{21}	$\delta(C_mH)$	1139	1172	1119	1142	1088	1122	1145	1139	1144
ν_{22}	ν(Pyr half-ring)$_{asym}$	1005	1032	1002	1006	906	1007	1015	1005	1015
ν_{24}	δ(Pyr def)$_{asym}$	806	817	794	808	638	739	805	807	806
ν_{25}	δ(Pyr rot)	429	439	440	437	459	444	439	432	433
B_{2g}										
ν_{31}	$\nu(C_\beta H)_{asym}$		3241	3095	3101	3109	3098	3101	3101	3101
ν_{27}	$\nu(C_mH)$		3212	3041	3073	3080	3073	3073	3073	3073
ν_{28}	$\nu(C_\alpha C_m)_{sym}$	1505	1550	1503	1504	1475	1478	1507	1505	1508
ν_{29}	ν(Pyr quarter-ring)	1368	1399	1363	1365	1402	1358	1356	1365	1356
ν_{34}	$\delta(C_\beta H)_{asym}$	1195	1229	1195	1193	1123	1195	1196	1196	1198
ν_{30}	ν(Pyr half-ring)$_{asym}$	1062	1087	1062	1062	954	1070	1071	1063	1070
ν_{32}	δ(Pyr def)$_{asym}$	819	833	826	825	734	811	827	821	829
ν_{33}	δ(Pyr rot)	435	442	420	427	376	438	415	408	418
ν_{35}	δ(Pyr trans)		244	198	232	283	214	216	235	210
E_u										
ν_{43}	$\nu(C_\beta H)_{sym}$		3261	3100	3120	3114	3113	3110	3110	3110
ν_{45}	$\nu(C_\beta H)_{asym}$		3241	3095	3101	3109	3098	3101	3101	3101
ν_{36}	$\nu(C_mH)$		3212	3041	3073	3080	3073	3073	3073	3073
ν_{37}	$\nu(C_\alpha C_m)_{asym}$	1592	1640	1580	1595	1701	1600	1604	1593	1604
ν_{38}	$\nu(C_\beta C_\beta)$	1547	1600	1551	1558	1567	1532	1548	1548	1547
ν_{39}	$\nu(C_\alpha C_m)_{sym}$	1462	1513	1470	1467	1417	1477	1480	1463	1480
ν_{40}	ν(Pyr quarter-ring)	1385	1427	1377	1397	1393	1396	1381	1383	1380
ν_{41}	ν(Pyr half-ring)$_{sym}$	1319	1358	1331	1322	1344	1346	1325	1320	1325
ν_{51}	$\delta(C_\beta H)_{asym}$	1250	1292	1271	1263	1240	1289	1275	1253	1274
ν_{42}	$\delta(C_mH)$	1150	1183	1132	1151	1099	1136	1144	1149	1145
ν_{52}	$\delta(C_\beta H)_{sym}$	1064	1092	1058	1061	1040	1063	1063	1061	1063
ν_{44}	ν(Pyr half-ring)$_{asym}$	1037	1062	1031	1037	937	1035	1034	1037	1034
ν_{47}	ν(Pyr breathing)	995	1023	1010	993	874	988	993	995	993
ν_{46}	δ(Pyr def)$_{asym}$	806	816	813	806	699	774	808	807	809
ν_{48}	δ(Pyr def)$_{sym}$	745	758	740	746	606	734	745	744	746
ν_{50}	ν(NiN)	420	420	429	411	435	461	424	412	416
ν_{49}	δ(Pyr rot)	366	378	363	371	366	341	351	378	342
ν_{53}	δ(Pyr trans)	289	306	283	293	283	282	316	284	319
					Out-of-Plane					
B_{1u}										
γ_{10}	$\gamma(H_mC_\alpha C_mC_\alpha)$		917		891	894	894	893	893	891
γ_{11}	Pyr fold$_{asym}$		850		829	840	839	839	839	840
γ_{12}	Pyr swivel		699		693	683	681	682	680	687
γ_{13}	$\gamma(C_mC_\alpha C_mC_\alpha)$		469		460	440	441	436	436	446
γ_{14}	ruffle		39		17	69	81	74	72	64
A_{1u}										
γ_1	Pyr fold$_{asym}$		684		677	662	660	655	658	673
γ_2	$\gamma(H_\beta C_\beta - C_\beta H_\beta)_{asym}$		910		882	890	889	89	889	888
γ_3	propeller		274		271	292	272	281	282	280

TABLE 2 (Continued)

	mode	expt[a]	B3LYP/6-31G(d,p)[b]	NMA[c]	SQM[c]	DIAG	STDX	NSTDX	CIPX	TORX
					Out-of-Plane					
B_{2u}										
γ_{15}	Pyr fold$_{sym}$		653		652	655	644	644	645	651
γ_{16}	Pyr tilt		239		259	254	258	253	255	249
γ_{17}	$\gamma(H_\beta C_\beta - C_\beta H_\beta)_{sym}$		794		780	787	784	785	785	781
γ_{18}	saddle		37		43	74	71	71	72	28
A_{2u}										
γ_4	$\gamma(H_m C_\alpha C_m C_\alpha)$	854	869		855	845	843	843	843	845
γ_5	Pyr fold$_{sym}$	768	775		767	788	785	786	785	780
γ_7	$\gamma(C_m C_\alpha C_m C_\alpha)$	698	707		705	704	704	705	703	695
γ_6	Pyr tilt	357	349		368	335	345	345	343	358
γ_8	$\gamma(H_\beta C_\beta - C_\beta H_\beta)_{sym}$	282	264		282	240	254	249	257	254
γ_9	dome	108	104		107	46	37	37	36	116
E_g										
γ_{19}	$\gamma(H_m C_\alpha C_m C_\alpha)$	844	860		842	842	841	841	841	842
γ_{20}	Pyr fold$_{asym}$	776	786		773	786	784	785	784	781
γ_{21}	Pyr fold$_{sym}$	896	915		888	892	891	891	891	890
γ_{22}	Pyr swivel	418	436		420	408	400	403	395	410
γ_{23}	Pyr tilt	656	671		662	655	654	651	652	660
γ_{24}	$\gamma(C_m C_\alpha C_m C_\alpha)$		704		700	697	702	699	698	697
γ_{25}	$\gamma(H_\beta C_\beta - C_\beta H_\beta)_{sym}$		231		229	247	243	243	243	238
γ_{26}	wave		139		141	179	178	178	178	152

[a] The experimental values are from ref 18. Solid samples were used for measurement of both IR (CsI and KBr pellets) and Raman (polycrystalline samples) spectra. [b] The frequencies from density functional calculations were performed in this study. [c] The NMA and SQM frequencies are from ref 18.

Nonbonding Interactions. Nonbonding (E^{nb}) interactions such as van der Waals, electrostatic and hydrogen bonding, are important in molecular interactions. The calculations reported here included van der Waals interactions (Table 3), though their influence should be minimal. Hydrogen bonding and electrostatics were omitted. NiP has no atoms available for hydrogen bonding, and ignoring electrostatics has been validated in previous studies.[53]

Levels of Treatment (Force Fields). To systematically examine the effects of cross terms upon the quality of the classical force field, five different force fields were studied. These force fields were fit to the same $\mathbf{H}^{expt}$.

(1) *DIAG*: Only diagonal terms and van der Waals nonbonding interactions are included. All cross terms are omitted.

(2) *STDX*: In addition to all of the terms in DIAG, this force field incorporates all standard (1,2) cross terms.

(3) *NSTDX*: This force field includes all of the diagonal and (1,2) terms in STDX as well as nonstandard (1,3) cross terms.

(4) *CIPX*: This level incorporates all terms in NSTDX as well as all other, longer range, in-plane cross terms for heavy-atom motions (except those involving the Ni−N stretch).

(5) *TORX*: This force field includes all NSTDX terms along with the torsion−stretch and torsion−bend cross terms.

Fitting the Classical Force Field. Once a set of force field terms was chosen, it was fit to the measured geometry and $\mathbf{H}^{expt}$ using singular value decomposition (SVD) least-squares fitting.[54] Because the force constants and geometry are usually entangled, the procedure adopted an iterative-switching approach in which the geometry and force constants are fit alternately. Symmetry was not employed.

To balance fitting of the geometry and Hessian, the procedure allowed for adjustable weighting of elements in the force vector and the $\mathbf{H}^{expt}$ matrix:[35−37]

$$\mathrm{Err} = \left[\frac{W_F^2}{N_F}\right]\sum_{i=1}^{3N}[w_F^i(\delta E_i')]^2 + \left[\frac{W_H^2}{N_H}\right]\sum_{i\geq j}^{3N}[w_H^{ij}(\delta E_{ij}'')]^2 \qquad (3)$$

N_H and N_F are normalization factors. $\delta E'$ and $\delta E''$ are errors in the force and Hessian matrixes, respectively. All force fields were generated using global weighting factors $W_F = 10.0$ and $W_H = 1.0$. No special weighting of individual elements was employed (i.e., $w_F^i = w_H^{ij} = 1.0$).

Several improvements have been made to the published method. One of the most time-consuming steps is calculating the Jacobian matrix, which contains the derivatives of the errors. To improve the speed of this computationally intensive step, the force constant portion of the Jacobian matrix was computed analytically rather than numerically. The coordinate portion was still calculated numerically, but a new, bi-phasic approach improved speed without sacrificing accuracy. Initially, the faster, less accurate finite-difference method was used; the final steps used the slower, more accurate Ridder's algorithm.[54]

Unfortunately, some advantages inherent in SVD fitting were lost in the treatment of this highly redundant system. Though SVD still removed ill conditions, for the larger system, the method could no longer indicate which force field terms were important and which were not.

In this study, the force fields were fit to only the natural abundance $\mathbf{H}^{expt}$ and the experimental geometry. No refinement of force constants with a final fit directly to fundamental frequencies was employed. This omission may decrease the accuracy of the final frequencies, but the physical meaning of the force constants is maintained. Further, spectra of isotopomers were not used as fitting parameters. Rather, they were used to test the reliability of the final results. These two approaches keep the calculation relatively simple, but still realistic.

III. Results and Discussion

Five force fields differing in complexity were made for NiP (Figure 1). These were fit to the NiP crystal structure,[44] and an $\mathbf{H}^{expt}$ derived from DFT (B3LYP/6-31G(d,p)) and experimental spectra.[18] The DIAG force field consists of only diagonal terms. AMBER[55−60] and OPLS[60−64] are commercially available force fields of the same approximate complexity as DIAG. STDX has the complexity generally used in commercial force fields such as CVFF,[60,65] for example. It contains only the shortest

TABLE 3: Potential Energy Terms in the HBFF-SVD Force Fields

Diagonal Terms:	
Stretch	$E_s = \frac{1}{2}K_s(r-r_e)^2$
Bend	$E_b = \frac{1}{2}F_b(\cos\theta - \cos\theta_e)^2$; $F_b = 1/K_b \sin^2\theta_e$
Torsion	$E_t = \sum_{n=1}^{3} V_n \cos(n\phi)$
Standard Cross-terms:	
1,2 Stretch-Stretch *(three-atom term)* 	$E^{1,2}_{r,r'} = K^{1,2}_{r,r'}(r_1 - r_1^e)(r_2 - r_2^e)$
1,2 Stretch-Bend *(three atom term)* 	$E^{1,2}_{\theta r} = F^{1,2}_{\theta r}(\cos\theta_2 - \cos\theta_2^e)(r_1 - r_1^e)$; $F^{1,2}_{\theta,r} = -1/K^{1,2}_{\theta,r}\sin\theta_2^e$
1,2 Bend-Bend *(four atom term)* 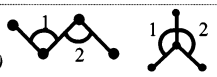	$E^{1,2}_{\theta,\theta'} = F^{1,2}_{\theta,\theta'}(\cos\theta_1 - \cos\theta_1^e)(\cos\theta_2 - \cos\theta_2^e)$; $F^{1,2}_{\theta,\theta'} = 1/K^{1,2}_{\theta,\theta'}\sin\theta_1^e \sin\theta_2^e$
Non-standard Cross-terms:	
1,3 Stretch-Stretch *(four atom term)* 	$E^{1,3}_{r,r} = K^{1,3}_{r,r}(r_1 - r_1^e)(r_2 - r_2^e)$
1,3 Bend-Bend *(five atom term)* 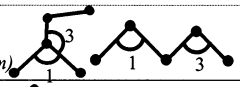	$E^{1,3}_{\theta,\theta'} = F^{1,3}_{\theta,\theta'}(\cos\theta_1 - \cos\theta_1^e)(\cos\theta_3 - \cos\theta_3^e)$; $F^{1,3}_{\theta,\theta\theta} = 1/K^{1,3}_{\theta,\theta\theta}\sin\theta_1^e \sin\theta_3^e$
1,3 Stretch-Bend *(four atom term)* 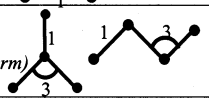	$E^{1,3}_{\theta r} = F^{1,3}_{\theta r}(\cos\theta_3 - \cos\theta_3^e)(r_1 - r_1^e)$; $F^{1,3}_{\theta,r} = -1/K^{1,3}_{\theta,r}\sin\theta_3^e$
Torsion (in-plane – out-of-plane) Cross-terms:	
Torsion-Stretch *(four atom term)* 	$E_{r\phi} = \sum_{n=0}^{3} V'_{mn}\cos(n\phi)(r_m - r_m^e)$
Torsion-Bend *(four atom term)* 	$E_{\theta\phi} = \sum_{n=0}^{3} V''_{mn}\cos(n\phi)(\cos\theta_m - \cos\theta_m^e)$; $V''_{mn} = -1/K''_{mn}\sin\theta_m^e$
Non-bonding Interactions:	
van der Waals	$E_{vdw} = \varepsilon_{ij}\left[2(\frac{\sigma_{ij}}{r_{ij}})^9 - 3(\frac{\sigma_{ij}}{r_{ij}})^6\right]$

TABLE 5: Analysis of Isotope Substitution Results; Comparison of HBFF-SVD Force Fields, DFT, NMA, and SQM

rms error[a]	B3LYP/6-31G(d,p)[b]	NMA[c]	SQM[c]	H^{exp}	STDX	NSTDX	CIPX	TORX
Δd_4								
in-plane	4.8	13.7	4.0	4.1	7.9	5.9	5.1	5.5
out-of-plane	4.4		4.8	3.0	7.0	6.0	6.4	6.5
total	*4.7*	*13.7*	*4.2*	*3.9*	*7.7*	*6.0*	*5.4*	*5.7*
Δd_8								
in-plane	8.1	89.2	4.6	7.9	12.7	10.7	8.3	10.5
out-of-plane	5.0		5.6	4.2	7.7	8.1	8.6	4.6
total	*7.6*	*89.2*	*4.8*	*7.3*	*11.9*	*10.2*	*8.3*	*9.7*
Δd_{12}								
in-plane	25.2	67.8	5.7	5.1	12.0	6.8	5.4	6.9
out-of-plane	3.2		6.4	5.0	15.3	15.4	16.0	12.9
total	*24.0*	*67.8*	*5.8*	*5.1*	*12.3*	*8.0*	*7.1*	*7.7*

[a] Rms errors (cm^{-1}) were computed by comparison to experimentally available frequencies (ref 18). Each frequency associated with a doubly degenerate pair of modes was counted twice to ensure balance in error analysis over the whole $3N - 6$ vibrational space. As described in the text, isotope assignments likely to be erroneous were omitted from the error analysis. For Δd_4, Δd_8, and Δd_{12}, the number of experimental frequencies used in rms error computation was 52, 49, and 44, respectively. [b] The density functional calculation was performed in this study. [c] The NMA and SQM analyses used frequencies from ref 18.

range (1,2) cross terms. NSTDX contains an expanded set of cross terms, with longer range (1,3) interactions as well as those in STDX. Traditional NMA usually includes a selected subset of 1,3 interactions, placing its complexity somewhere between STDX and NSTDX. Finally, we also explored the need for longer range, in-plane, cross terms (CIPX) and for explicit coupling of in-plane and out-of-plane degrees of freedom (TORX).

Fitting yielded force constants and equilibrium geometry parameters. These were used to calculate vibrational frequencies for the naturally abundant (Figure 2; Tables 2 and 4) and isotopically labeled (Table 5) NiP. Three isotopically labeled NiPs were examined: d_4 (meso positions deuterated), d_8 (β positions deuterated), and d_{12} (all peripheral positions deuterated). The isotope shifts are an independent and stringent test of the force fields, as these data were not used in the fit. Below,

TABLE 4: Analysis of Natural Abundance Spectra Results; HBFF-SVD Force Fields Compared to DFT, NMA, and SQM

rms error[a]	B3LYP/6-31G(d,p)[b]	BLYP/6-31G(d,p)[b]	NMA[c]	SQM[c]	DIAG	STDX	NSTDX	CIPX	TORX
A_{1g} modes	37.37	12.91	7.48	7.01	87.31	28.20	13.99	1.96	14.16
B_{1g} modes	37.80	11.20	23.67	8.90	72.12	16.86	11.93	2.71	14.60
A_{2g} modes	33.21	10.32	11.81	5.88	82.30	20.09	11.33	1.43	11.17
B_{2g} modes	28.98	15.95	7.11	4.36	70.38	12.50	10.60	10.92	10.04
E_u modes	33.49	9.48	10.63	6.40	70.16	21.05	11.98	4.17	13.34
all in-plane	*34.14*	*11.09*	*12.83*	*6.65*	*74.25*	*20.72*	*12.03*	*4.80*	*13.08*
A_{2u} modes	11.23	20.87		5.37	33.15	32.54	33.51	32.78	13.55
E_g modes	15.89	20.78		4.84	6.54	9.06	8.55	11.51	5.34
all out-of-plane	*14.32*	*20.81*		*5.05*	*20.95*	*21.17*	*21.61*	*22.04*	*9.31*
all modes	*30.95*	*13.79*		*6.34*	*66.45*	*20.82*	*14.64*	*11.09*	*12.36*

[a] Rms errors (cm^{-1}) were computed by comparison to experimentally available frequencies. Experimental assignments have been reported (ref 18) for 58 in-plane modes (28 nondegenerate and $15 \times 2 = 30$ doubly degenerate) and 16 out-of-plane modes (6 nondegenerate and $5 \times 2 = 10$ doubly degenerate). Each frequency associated with a degenerate pair was counted twice to ensure balance in error analysis over the whole $3N - 6$ vibrational space. [b] The density functional calculations were performed in this study. [c] The NMA and SQM analyses used frequencies from ref 18.

we compare the force fields to one another, discuss important diagonal and off-diagonal force constants, and compare our findings to published NMA and SQM results.

Vibrational Frequencies (Natural Abundance). NiP (Figure 1) is one of the simplest metalloporphyrins, with hydrogens at all twelve peripheral sites. When treated as a D_{4h} symmetry molecule, its 105 vibrational modes consist of 71 in-plane ($\Gamma_{in-plane} = 9\ A_{1g} + 9\ B_{1g} + 8\ A_{2g} + 9\ B_{2g} + 18\ E_u$) and 34 out-of-plane ($\Gamma_{out-of-plane} = 5\ B_{1u} + 3\ A_{1u} + 4\ B_{2u} + 6\ A_{2u} + 8\ E_g$) degrees of freedom. Of these, 74 have been experimentally determined[18] (34 nondegenerate and $20 \times 2 = 40$ doubly degenerate) (Table 2). A_{1g}, B_{1g}, A_{2g}, and B_{2g} modes are enhanced in Raman spectra in resonance with the major $\pi-\pi^*$ absorption bands (B and Q bands). Though the E_g modes are also Raman active, they are not enhanced by the B and Q band transitions. However, NiP is slightly distorted along the ruffling coordinate (Figure 1) in the crystal, and probably in solution as well. This lowering of molecular symmetry to D_{2d} alters the selection rules. The E_g modes become slightly IR active, and the five highest frequency ones have been recently assigned.[18] The E_u and A_{2u} modes are also IR active.

Porphyrin normal modes can be described in dominant local coordinate components, as discussed thoroughly in the literature (for a review, see ref 2). Both local and normal designations are used here. Mode numbering is consistent with the designations given by Kitagawa and co-workers for Ni octaethylporphyrin (Table 2).[7,9] D_{4h} notation is used in this study.

As discussed above, experimental frequencies were used to form $\mathbf{H}^{expt}$ in the HBFF-SVD procedure. The different force fields (DIAG, STDX, NSTDX, CIPX, TORX) were then fit to this matrix. Where no experimental frequency was available, results from SQM[18] were used. However, all evaluations of force field accuracy utilized only the experimental values. Experimental data have been reported for the natural abundance NiP for 58 in-plane modes (28 nondegenerate and $15 \times 2 = 30$ doubly degenerate modes) and 16 out-of-plane modes (6 nondegenerate and $5 \times 2 = 10$ doubly degenerate modes).

DIAG. The simplest force field, with no cross terms, performed quite poorly in calculating frequencies. The potential near the minimum was fit so badly that many modes were very difficult to assign. The rms error was 66 cm^{-1}, with a larger overall error in the in-plane motions (74 cm^{-1}); nearly 30 of the modes differed from their experimental frequencies by over 50 cm^{-1}. This inadequate performance for the DIAG force field is not unexpected. It is well-known that although this level of complexity can reproduce geometries with accuracy, it is insufficient for accurately calculating delocalized vibrational frequencies.

STDX. Adding the shortest range cross terms (1,2 stretch−stretch, 1,2 stretch−bend, and 1,2 bend−bend) led to remarkable improvement. These three- and four-atom terms reduced the rms error to 20.8 cm^{-1}, with dramatic improvement for some modes. Virtually all improvement was in the in-plane part of the force field (rms error = 20.7 cm^{-1}). The lack of improvement in the out-of-plane portion is explained by the absence of cross terms involving out-of-plane motions.

Though STDX is a great improvement over DIAG, the fidelity with which STDX reproduced the experimental frequencies was still relatively poor. Eighteen modes were in error by more than 20 cm^{-1}, and only thirteen were within 5 cm^{-1}. In particular, the in-plane Ni−N stretches (ν_8, ν_{18}, ν_{50}), $C_\alpha-C_m$ stretches (ν_3, ν_{10}, ν_{19}, ν_{28}, ν_{37}, and ν_{39}), and some of the pyrrole in-plane deformation modes (e.g., ν_7, ν_{24}, ν_{46}) exhibited fairly large deviations from experiment. The out-of-plane doming was calculated quite inaccurately, with an error of 70 cm^{-1}.

NSTDX. The 1,3 stretch−stretch, stretch−bend, and bend−bend interactions in the NSTDX force field improved the fit even further (total rms error = 14.6 cm^{-1}). These cross terms are all in-plane, and accordingly, the advances were seen there (in-plane rms error = 12.0 cm^{-1}). The NSTDX force field generated 17 frequencies within 2 cm^{-1} of their experimental values, and 30 within 5 cm^{-1}. The calculated out-of-plane frequencies possessed roughly the same degree and pattern of error as for DIAG and STDX.

Significant improvement was made in the Ni−N stretch frequencies. The absolute errors in ν_8, ν_{18}, and ν_{50} dropped from an average of 34 to 10 cm^{-1}. Examination of the modes indicated that the improvement comes largely from inclusion of 1,3-(Ni−N)−($C_\alpha-C_m$) stretch−stretch and 1,3-(Ni−N)−(N−$C_\alpha-C_m$) stretch−bend interactions. Residual errors in ν_8 and ν_{18} appeared to arise from significant untreated components of $C_\alpha-C_m-C_\alpha$ and $C_\beta-C_\alpha-C_m$ bends, respectively.

The $C_\beta-C_\beta$ stretches (ν_2, ν_{11}, and ν_{38}) improved greatly as well. The absolute average error in these modes went from 15 to 3 cm^{-1} with the addition of 1,3 cross terms. These modes were fit relatively well with STDX because there are several 1,2 stretch−bend (e.g., ($C_\beta-C_\beta$)−($C_\beta-C_\beta-C_\alpha$), (C_α−N)−(C_α−N−C_α), and (C_α−N)−(C_α−N−C_β)) and 1,2 bend−bend (e.g., ($C_\beta-C_\beta-C_\alpha$)−($C_\beta-C_\alpha$−N) and ($C_\beta-C_\beta-C_\alpha$)−($C_\beta-C_\alpha-C_m$)) interactions involved in the pyrrole distortion that accompanies the large $C_\beta-C_\beta$ stretching. The improvement in NSTDX appeared to come largely from 1,3 stretch−stretch coupling of ($C_\beta-C_\beta$) with (C_α−N) and ($C_\alpha-C_m$). Residual error in ν_2 was probably from $C_\alpha-C_m-C_\alpha$ bend components, the coupling of which to ($C_\beta-C_\beta$) requires longer range cross terms.

The $C_\alpha-C_m$ stretches (ν_3, ν_{10}, ν_{19}, ν_{28}, ν_{37}, ν_{45}) showed only

moderate improvement, from an average absolute error of 20 cm^{-1} in STDX to 15 cm^{-1} in NSTDX. Our studies thus agree with previous analyses that longer range terms are required to adequately fit these modes.[13]

CIPX. Though the inclusion of the 1,3 type cross terms in the NSTDX force field improved the calculated frequencies considerably, room for improvement remained in several modes. Rather than introduce bias by selecting couplings, we included these longer range force constants in the form of a complete in-plane force field (CIPX). Though this force field may not be practical for use in molecular mechanics calculations, it can lend insight into longer range coupling required to accurately fit the vibrational space of this large conjugated system.

All heavy-atom binary cross terms of the stretch−stretch, stretch−bend and bend−bend type were included, except those involving the Ni−N bonds. Long range bend−bend interactions involving hydrogens were included as well. The resultant improvement in the in-plane frequencies was very good. A total of 51 of the 58 frequencies experimentally available were fit within 5 cm^{-1} of their experimental values, and only three modes were greater than 10 cm^{-1} in error. The overall rms error was improved to 11.1 cm^{-1}, with only 4.8 cm^{-1} rms error in the in-plane modes. As expected, no improvement was observed in the out-of-plane degrees of freedom.

TORX. All of the improvements garnered by the above force fields were in-plane. The out-of-plane coordinates were explored as well, though the experimental frequencies are sparse, through coupling in-plane and out-of-plane degrees of freedom. In TORX, this coupling occurs through cross terms between torsions and the bends and stretches occurring within them.

These cross terms did not improve the in-plane force field. The in-plane rms error went from 12 cm^{-1} in NSTDX to 13 cm^{-1} for TORX. TORX did, however, more accurately reproduce out-of-plane vibrations. The rms error for out-of-plane motions was around 21 cm^{-1} for all of the force fields employed except TORX, where it was 9.3 cm^{-1}. Most improvement was seen in the A_{2u} dome mode γ_9, which was underestimated by about 70 cm^{-1} in STDX, NSTDX, and CIPX. This low-frequency mode (expt = 108 cm^{-1}) was calculated by TORX only 8 cm^{-1} from experiment. Other out-of-plane modes improved slightly as well, suggesting that out-of-plane and in-plane couplings should not be ignored in treating the out-of-plane modes. The largest error remained in the A_{2u} mode γ_8, assigned by Spiro and co-workers to a symmetric ($HC_\beta-C_\beta H$) distortion. Our examination of the mode showed that it has a large component of Ni out-of-plane doming motion. The coupling of these two out-of-plane motions is not present in our force field.

In summary, DIAG reproduced most modes poorly. STDX and NSTDX include short (1,2) and longer (1,3) range terms that account for resonance-type effects, and significantly improved the accuracy of most in-plane motions. The CIPX force field couples almost all heavy-atom, in-plane motions, and accounts for longer range resonance effects. The improvement in fit was dramatic, with rms error for in-plane modes of only 5 cm^{-1}. The aromaticity of the NiP macrocycle requires the long range cross terms for accurate modeling of the vibrational structure.

As expected, the accuracy of fitting out-of-plane modes was similar for DIAG, STDX, NSTDX, and CIPX, as all used the same out-of-plane force field. In contrast, the TORX force field, which includes in-plane and out-of-plane coupling, improved the treatment of out-of-plane motions. Thus, examination of interactions among out-of-plane degrees of freedom is warranted.

Isotope Shifts. In this study, isotope shift data were used to evaluate the ability of the new force fields to accurately represent the NiP potential surface near the minimum. The isotope shifts were not used in optimizing the force fields. Three deuterium substitutions were examined: at the four meso positions (NiP-d_4), at the eight β-positions (NiP-d_8), and at all twelve peripheral sites (NiP-d_{12}). Experimental data are available and assignments have been made for these species.[18] Table 5 contains a summarized error analysis.

In principle, the upper limit on the accuracy of the HBFF-SVD force fields is determined by the $\mathbf{H}^{expt}$. The total rms errors for $\mathbf{H}^{expt}$ for the NiP-d_4, NiP-d_8, and NiP-d_{12} isotopomers were 3.9, 7.3, and 5.1 cm^{-1}, respectively. Errors were relatively balanced between the in-plane and out-of-plane distortions, though the in-plane motions were fit somewhat more poorly for all three deuterated species.

With the exception of DIAG, the HBFF-SVD force fields also reproduced the isotope shifts with good accuracy. DIAG was not evaluated as reliable assignments could not be made. The least accurate force field was STDX, with total rms errors of 7.7, 11.9, and 12.3 cm^{-1} for NiP-d_4, -d_8, and -d_{12}, respectively. The addition of the 1,3 and longer range cross terms led to improvement for NSTDX (total rms error for NiP-d_4 = 6.0 cm^{-1}, NiP-d_8 = 10.2 cm^{-1}, and NiP-d_{12} = 8.0 cm^{-1}) and CIPX (total rms error for NiP-d_4 = 5.4 cm^{-1}, NiP-d_8 = 8.3 cm^{-1}, and NiP-d_{12} = 7.1 cm^{-1}). None of the HBFF-SVD force fields reproduced the experimental isotope-shifted frequencies as well as direct diagonalization of $\mathbf{H}^{expt}$, suggesting that improvement in the fitting is possible. However, there is not much room for improvement: NSTDX was less than 3 cm^{-1} in total rms error from the limit set by $\mathbf{H}^{expt}$, and CIPX was less than 2 cm^{-1} from this limit.

The HBFF-SVD results suggest that some of the assignments of isotopically shifted bands may be in error. Although no reassignments were made for the natural abundance spectrum, a couple of assignments of isotope shift bands were regarded as doubtful, and therefore ignored in the rms error evaluation. One was the B_{1g} mode ν_{12} for NiP-d_8. The experimental assignment for this mode indicated a shift of 59 cm^{-1},[18] whereas the HBFF-SVD results showed a shift of only 1−3 cm^{-1} with $\mathbf{H}^{expt}$ and all force fields. We suggest that this is an error in the experimental assignment. The position of ν_{12} is shifted by 62 cm^{-1} in NiP-d_4.[18] To first order, one would expect a shift of over 100 cm^{-1} for the NiP-d_{12} ν_{12} if the d_8 shift is really 59 cm^{-1}. The experimentally reported value is 68 cm^{-1}, however.[18] Were this the only argument, we would not have it felt sufficient to doubt this assignment. However, examination of the normal mode displacements from our calculations supported this suggestion (not shown); the mode clearly shifted for d_4 and d_{12}, but not for NiP-d_8. NMA predicted a shift of only 13 cm^{-1} for this mode,[18] whereas SQM predicted a shift of 66 cm^{-1}.[18] Given the controversy, we felt justified in omitting this piece of data from the error assessment. The reported experimental shift of 12 cm^{-1} for the ν_{40} E_u mode in NiP-d_4 was ignored as well for similar reasons. The shift was not reported for NiP-d_4 and -d_{12} and disagreed with both our results and the SQM findings.[18]

One side product of the HBFF-SVD method is that the experimentally corrected Hessian, $\mathbf{H}^{expt}$, provides an excellent tool for experimental assignment of isotope shifts. Comparison with the experimental assignments in NiP showed that the $\mathbf{H}^{expt}$-predicted shifts were significantly more accurate than DFT's. Though DFT did fairly well in predicting the isotope shifts, a

TABLE 6: Selected Force Field Equilibrium Geometry Parameters for Ni Porphine

	DIAG	STDX	NSTDX	CIPX	TORX
		Bond Lengths (Å)			
Ni−N	1.9383	1.9357	1.9348	1.9333	1.9405
C_α−N	1.3777	1.3783	1.3776	1.3779	1.3793
C_α−C_β	1.4363	1.4351	1.4348	1.4339	1.4386
C_α−C_m	1.3738	1.3732	1.3724	1.3728	1.3814
C_β−C_β	1.3496	1.3492	1.3491	1.3480	1.3585
rms error[a]	*0.0060*	*0.0070*	*0.0074*	*0.0081*	*0.0084*
		Bond Angles (deg)			
N−Ni−N	90.0	90.0	90.0	90.0	90.0
Ni−N−C_α	127.6	127.6	127.7	127.7	127.7
C_α−N−C_α	104.8	104.7	104.7	104.6	104.6
N−C_α−C_β	110.8	110.7	110.8	110.9	111.1
N−C_α−C_m	125.0	125.1	125.0	125.0	125.0
C_m−C_α−C_β	124.1	124.0	124.1	124.0	123.7
C_α−C_β−C_β	106.9	106.9	106.8	106.9	106.6
C_α−C_m−C_α	123.3	123.1	123.3	123.2	123.0
rms error[a]	*0.3*	*0.3*	*0.3*	*0.3*	*0.3*
		Ruffling Angle (deg)			
C_α−N- - -N−C_α	22.4	22.8	22.8	22.5	23.7

[a] The reported rms errors are relative to the X-ray crystal structure values from ref 44 and listed in Table 1.

TABLE 7: Diagonal Force Constants for HBFF-SVD and NMA Force Fields

	DIAG	STDX	NSTDX	CIPX	TORX	NMA[a]
			Bond Stretches [kcal/(mol Å^2)]			
C_β−C_β	977.51	1191.46	1092.62	1075.76	1088.93	1057.20
C_α−C_m	855.39	1056.92	977.21	978.47	984.50	996.96
C_α−N	598.82	868.82	822.12	824.24	823.02	846.57
C_α−C_β	599.72	793.35	753.65	746.86	753.50	781.00
Ni−N	248.06	287.94	241.20	241.86	239.69	270.30
C_β−H	756.92	759.32	759.48	759.48	759.47	747.65
C_m−H	743.11	746.68	746.44	746.42	746.46	721.77
			Angle Bends [kcal/(mol rad^2)]			
C_α−N−C_α	184.85	215.44	213.07	201.68	209.86	213.80
N−C_α−C_β	108.98	190.98	207.90	204.52	207.50	241.12
C_α−C_β−C_β	137.05	145.59	167.31	164.02	169.42	179.00
C_α−C_m−C_α	86.88	111.41	128.91	128.52	125.06	180.15
N−C_α−C_m	81.40	67.63	73.53	72.74	72.17	104.10
C_β−C_α−C_m	95.16	71.05	73.16	72.80	73.16	104.10
N−Ni−N	192.38	68.70	54.92	58.79	50.65	52.34
Ni−N−C_α	101.24	35.66	26.46	25.98	22.99	34.79
C_α−C_β−H	57.05	46.83	48.79	48.90	49.72	65.56
C_β−C_β−H	60.76	39.96	44.67	43.70	45.60	65.56
C_α−C_m−H	70.76	39.27	54.39	52.27	56.12	68.29

[a] The NMA force constants are from ref 18.

few modes were not reproduced well, even at the relatively high level employed here.

The value of $\mathbf{H}^{expt}$ guidance is 2-fold. First, it is independent; the isotope data have not been used to optimize it in any way. Second, because $\mathbf{H}^{expt}$ does well with isotope shifts, and diagonalization of $\mathbf{H}^{expt}$ yields the experimental natural abundance frequencies exactly, the absolute experimental frequencies of the isotopically substituted species (i.e., not just the isotope shifts) are accurately predicted by diagonalization of $\mathbf{H}^{expt}$ with the isotope masses. Assignment of isotope substitution data would be tremendously simplified using this $\mathbf{H}^{expt}$-guided approach.

The Force Fields: Geometry. The equilibrium geometry parameters {r_0, θ_0, etc.} are determined during the HBFF-SVD fitting process. They were found to be very close to the experimental values at all levels of force field (Table 6). This result is not particularly surprising, given that a diagonal force field is sufficient to accurately calculate the molecular geometry. The rms difference in bond lengths ranged from 0.006 to 0.0084 Å, and the rms difference in bond angles was less than 0.5°. The bond lengths and angles did not exactly match the crystal structure because the HBFF-SVD method fits to both the geometry (forces = 0) and the $\mathbf{H}^{expt}$.

The only significant differences between the equilibrium and experimental[44] geometries were the ruffling angle (τ_{ruf}) (Figure 1) and Ni−N bond length. All HBFF-SVD force fields had ruffled structures ($\tau_{ruf} \sim 23°$) and shorter Ni−N bond lengths (~1.93−1.94 Å) (Table 6), whereas the X-ray structure is nearly planar with a longer Ni−N bond (1.951 Å) (Table 1). The differences reflect a problem with the functional form of the torsion potential in the HBFF-SVD force fields (Table 3) and the conflicting geometries observed in the crystal and DFT optimized structures. (A discussion of the difference between the DFT and X-ray geometries is present in the Computational Methods section.) Unlike the stretch and bend potential functions, which contain equilibrium lengths and angles, the Fourier expansion used for torsions contains no equilibrium angle. Thus the force vector contains no equilibrium torsion angles. Interestingly, regardless of whether the HBFF-SVD force field fitting was initiated using the B3LYP/6-31G(d,p) optimized structure or the crystal structure, the result was equilibrium geometry parameters reflecting a ruffled minimum with a shorter Ni−N bond length (not shown). Increasing the weighting for fitting the forces (W_F in eq 3) by a factor of 10 did not change the result (not shown). In fact, the only way to ensure planar equilibrium geometry parameters was to avoid fitting to the $\mathbf{H}^{expt}$ at all and fit to only the forces (not shown). In other words, in the absence of information about torsion in the force vector, the equilibrium torsion angle information present in the $\mathbf{H}^{expt}$ matrix dominates the results and produces similar ruffling angles at the DFT value for all HBFF-SVD force fields.

The Force Fields: Force Constants. All of the diagonal bond-stretch and angle-bend force constants are reported in Table 7, and a subset of cross terms are listed in Tables 8 and 9. Equivalent force constants from NMA[18] are included, where appropriate, though care should be exerted in direct comparison (see below).

Examination of Table 7 shows that the HBFF-SVD diagonal force constants are reasonable in both sign and magnitude. The C_β−C_β bond-stretch force constant is the largest, consistent with its larger double bond character. The Ni−N bond-stretch force constant is the smallest, as it should be for this weakest bond. The angle-bend force constants are generally large for motions that would distort the pyrrole ring. The C_α−C_m−C_α force constant is nearly as large, but the others are significantly smaller. The torsion force constants have been included in the Supporting Information. The V_2 component is the largest, reflecting the conjugated nature of the macrocycle. Generally, V_3 is larger than V_1 for a given torsion term. The largest torsional force constants involve motions about the −C_α−C_m− bond; the smallest involve motions about −N−Ni−.

The inclusion of cross terms led to small changes in all of the diagonal force constants except for bond stretches involving H. The largest percentage change was observed in going from DIAG to STDX. Consistently, the larger changes observed with increasing force field complexity were associated with motions involving the Ni−N bond. This finding probably derives from the geometry issues surrounding ruffling and the Ni−N distance discussed above.

Examination of the magnitudes and signs of the cross terms allows some physical insight into the porphyrin structure−spectrum relationship. (In the ensuing discussion, only bonds and angles involving heavy atoms are addressed. See Figure 1 for bond and angle labels.) For example, the 1,2 stretch−stretch

TABLE 8: Selected Stretch−Stretch Force Constants [kcal/(mol Å²)] for HBFF-SVD and NMA Force Fields

		STDX	NSTDX	CIPX	TORX	NMA[a]
1,2-						
$C_\alpha-N-C_\alpha$		210.49	67.49	62.24	73.42	79.08
$N-C_\alpha-C_m$		115.75	66.61	61.99	65.53	70.45
$C_\alpha-C_\beta-C_\beta$		131.81	66.10	66.87	64.47	69.01
$N-C_\alpha-C_\beta$		83.59	46.72	47.38	48.19	79.08
$C_\alpha-C_m-C_\alpha$		153.01	45.49	57.90	56.67	100.64
$C_\beta-C_\alpha-C_m$		96.50	41.38	33.73	42.62	86.27
$Ni-N-C_\alpha$		80.39	38.10	30.37	37.86	14.38
N−Ni−N		10.25	17.51	14.02	21.07	14.38
1,3-						
$(N-C_\alpha)-(C_\alpha-C_m)$ (trans)[b]			−47.42	−22.77	−46.83	−12.94
$(N-C_\alpha)-(C_\alpha-C_m)$ (cis)[b]			−45.56	−26.03	−38.85	−129.40
$(C_\alpha-C_m)-(C_\beta-C_\beta)$			−40.00	−29.69	−38.54	−33.07
$(C_\beta-C_\alpha)-(C_\alpha-C_m)$			−32.83	−26.37	−32.38	−37.38
$(Ni-N)-(C_\alpha-C_m)$			−23.99	−1.32	−27.56	17.25
$(N-C_\alpha)-(C_\beta-C_\beta)$			20.63	33.04	21.33	37.38
$(N-C_\alpha)-(C_\beta-C_\alpha)$			6.77	13.99	6.51	7.19
(Ni−N)−(N−C_α) (trans)[b]			4.83	15.09	5.73	17.25
(Ni−N)−(N−C_α) (cis)[b]			−0.86	0.62	−4.32	17.25
$(C_\beta-C_\alpha)-(C_\beta-C_\alpha)$			−4.26	3.18	−6.86	37.38
$(Ni-N)-(C_\beta-C_\alpha)$			−3.38	−7.44	−4.31	17.25
longer range	example					
1,4-						
$(C_\alpha-C_\beta)-(C_\alpha-C_m)$	(D1-G4)			28.64		
$(C_\alpha-C_\beta)-(N-C_\alpha)$	(E1-B2)			12.83		
$(C_\alpha-C_m)-(N-C_\alpha)$	(E1-F4)			13.83		
$(N-C_\alpha)-(N-C_\alpha)$	(E1-A2)			18.21		
1,5-						
$(C_\alpha-C_\beta)-(C_\alpha-C_m)$	(D1-F4)			−13.91		
$(N-C_\alpha)-(N-C_\alpha)$	(E1-E2)			10.24		
1,6-						
$(C_\alpha-C_m)-(C_\alpha-C_m)$	(F1-G2)			19.86		
$(C_\alpha-C_\beta)-(N-C_\alpha)$	(E1-D2)			14.15		
$(N-C_\alpha)-(N-C_\alpha)$	(E1-A4)			10.09		
1,7-						
$(N-C_\alpha)-(C_\alpha-C_m)$	(E1-G2)			12.91		
$(N-C_\alpha)-(C_\alpha-C_m)$	(E1-G3)			16.80		
1,8-						
$(C_\alpha-C_\beta)-(C_\alpha-C_m)$	(D1-G3)			11.77		
$(C_\alpha-C_m)-(C_\alpha-C_m)$	(F1-G3)			0.72		−24.44
1,9-						
$(C_\alpha-C_m)-(C_\alpha-C_m)$	(F1−F3)			25.82		24.44

[a] The NMA force constants are from ref 18. [b] Cis and trans refer to the arrangements of the atoms in the four-atom group.

TABLE 9: Significant Long Range Stretch−Bend and Bend−Bend Force Constants from the CIPX HBFF-SVD Force Field

stretch−bend	example	kcal/(mol Å rad)
$(C_\alpha-C_\beta)-(N-C_\alpha-C_m)$	(D1-i4)	−17.01
$(C_\alpha-C_m)-(N-C_\alpha-C_\beta)$	(G1-b1)	−22.27
	(G1-e3)	−18.06
$(C_\beta-C_\beta)-(C_\alpha-N-C_\alpha)$	(C1-a1)	33.15
$(C_\beta-C_\beta)-(Ni-N-C_\alpha)$	(C1-n1)	−22.26
$(C_\beta-C_\beta)-(N-C_\alpha-C_\beta)$	(C1-e2)	−16.05
	(C1-b3)	−15.73
$(N-C_\alpha)-(C_\beta-C_\alpha-C_m)$	(A1-j1)	−17.79

bend−bend	example	kcal/(mol rad²)
$(C_\beta-C_\alpha-C_m)-(C_\beta-C_\alpha-C_m)$	(g1-g3)	16.01
$(N-C_\alpha-C_\beta)-(C_\alpha-C_m-C_\alpha)$	(e1-h2)	16.98

interaction terms (STDX, NSTDX, CIPX) are all positive in value, whereas most of the 1,3 stretch−stretch couplings (NSTDX, CIPX) are negative. Positive stretch−stretch cross terms indicate that as one bond in the coupled pair is lengthened, the other tends to shorten. This can be readily seen by examining the stationary point along the first bond-stretch coordinate (r_1) of the energy $\{E = {}^1/_2k_1(r_1 - r_0)^2 + {}^1/_2k_2(r_2 - r_0)^2 + k_{12}(r_1 - r_0)(r_2 - r_0)\}$ as a function of the bond-stretch coordinate to which it is coupled (r_2):

$$r_1^{\min} = \left[\frac{k_1 + k_{12}}{k_1}\right] r_0 - \frac{k_{12}}{k_1} r_2 \qquad (4)$$

For simplicity, $k_1 = k_2$ and the equilibrium bond lengths for r_1 and r_2 are the same. In porphyrins, the positive 1,2 stretch−stretch and negative 1,3 stretch−stretch coupling constants reflects the conjugation around the macrocycle. Lengthening one bond reduces the conjugation, making the initially lengthened bond more single bond-like, its nearest neighbor more double bond-like, the 1,3 bond more single bond-like, and so forth. Figure 3 shows this sign alternation pattern for the coupling of the $C_\beta-C_\beta$ bond around the 18-membered conjugated ring. Other bond-bond coupling patterns can be seen in Figure 3 as well. Though the signs of the cross terms do not always alternate, the zigzag pattern is the same.

A few 1,3 stretch−stretch force constants are positive. Most involve coupling of $N-C_\alpha$ within the pyrrole ring (with $C_\beta-C_\beta$ and $C_\alpha-C_\beta$) or with Ni−N motions. These couplings are not in the conjugation pathway and are therefore fundamentally different types of interactions.

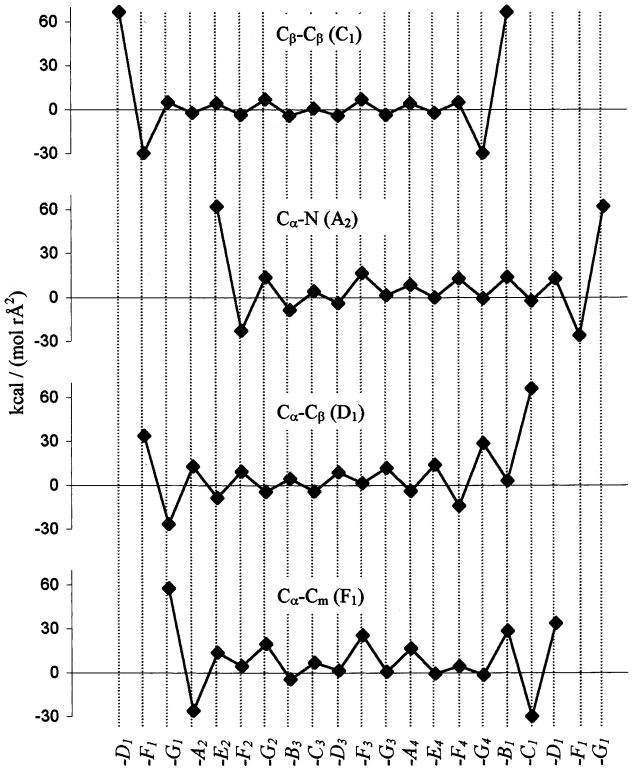

Figure 3. Stretch−stretch coupling about the conjugation path of NiP. The stretch−stretch interaction force constants from the CIPX force field in units of kcal/(mol Å^2) are plotted in a clockwise direction around the conjugation path depicted in Figure 1b. The bond labels correspond to those in Figure 1a.

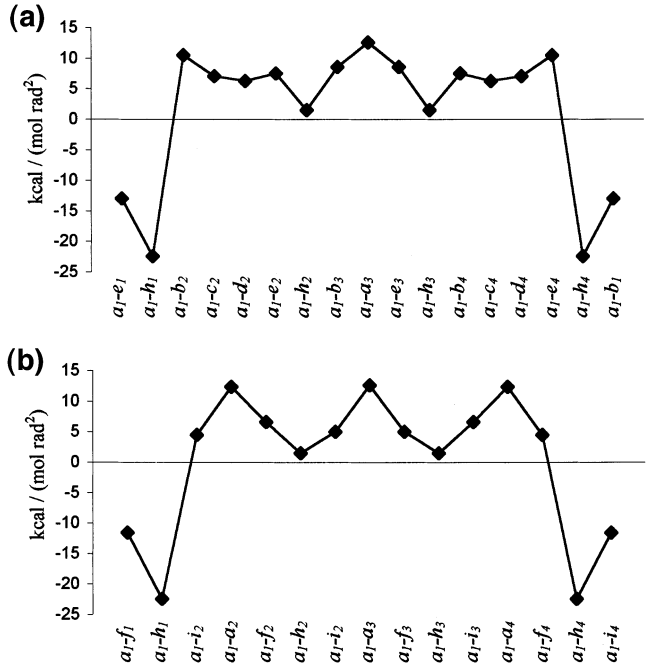

Figure 4. Bend−bend coupling of (Cα−N−Cα) about the conjugation path and the inner ring of NiP. The bend−bend interaction force constants from the CIPX force field in units of kcal/(mol rad^2) are plotted in a clockwise direction around the 18-membered conjugation path depicted in Figure 1b (Figure 4a) and about the 16-membered inner ring (Figure 4b). The angle labels correspond to those in Figure 1b.

The interpretation of the signs and magnitudes of the bend−bend coupling constants is analogous to that described above for stretch−stretch interactions. The aromatic nature of the bonding pattern does not translate into resonance structures with alternating strong and weak angles, as it does for the bonds (Figure 4). By symmetry, (Cα−N−Cα) is most similar to the Cβ−Cβ bond. Its coupling to its nearest neighbor (N−Cα−Cm) is large and negative; 1,3 bend−bend coupling to the next angle, Cα−Cm−Cα, is also negative, and larger in magnitude. All other angle−angle interactions with Cα−N−Cα about the conjugation pathway are positive. The pattern observed in the bend−bend cross terms indicates that the easiest way for the macrocycle to accommodate an angle opening at a single Cα−N−Cα is by opening the macrocycle near the perturbation, and narrowing it on the opposite side. This observation is borne out by the fact that the largest positive angle−angle coupling term is for the opposite Cα−N−Cα.

The coupling within a given pyrrole ring is quite interesting. With CIPX, all stretch−stretch interactions are positive, and all bend−bend interactions are negative. The only long range coupling terms are the three cross-pyrrole stretch−bend interactions, of which the (Cβ−Cβ)−(Cα−N−Cα) is the most significant. The interpretation of the signs of stretch−bend force constants is opposite from that of stretch−stretch and bend−bend interactions. Thus the large, positive value of this cross term (33 kcal/(mol Å rad)) indicates that increasing the Cβ−Cβ bond length is most easily accommodated by a concomitant increase in the Cα−N−Cα angle, which makes intuitive sense. It is noteworthy that this cross term is omitted from the NMA analysis (see below).

The intrapyrrole stretch−stretch interactions are of the 1,2 and 1,3 types, and their magnitudes cannot be accounted for by simple resonance arguments. The motion of the pyrrole is constrained by the rest of the macrocycle and the pyrroles in NiP participate in two types of conjugation: about the macrocycle and within the pyrrole. The resonance structures of the pyrroles in NiP and of an isolated pyrrole differ substantially. Comparison to the isolated pyrrole force field (not shown) indicates that the signs of the interactions are established mostly by the pyrrole itself, but the magnitudes are perturbed by the presence of the rest of the porphyrin ring.

The long range, binary couplings among stretches and bends over the NiP macrocycle also lend insight into the structure−spectrum relationship, particularly for this conjugated system. There are more than 300 unique, long range, stretch−stretch, stretch−bend, and bend−bend cross terms in the CIPX force field. A fairly large number of these, 83, were found to have absolute magnitudes larger than 10 kcal/(mol geom-unit); 68 are between 10 and 15 kcal/(mol geom-unit), 10 are between 15 and 20 kcal/(mol geom-unit), and 5 are quite large, with absolute magnitudes larger than 20 kcal/(mol geom-unit). The stretch−stretch terms above 10 kcal/(mol Å^2), and the stretch−bend and bend−bend terms above 15 kcal/(mol geom-unit), can be seen in Tables 8 and 9, respectively. A few of the more significant interactions are depicted in Figure 7.

The (Cβ−Cβ)−(Cβ−Cβ) pairs do not strongly interact, as observed previously.[13,16,18] These terms are all less than 1 kcal/(mol Å^2). In fact, the Cβ−Cβ bond does not couple strongly to any other distant bond. The largest long range stretch−stretch term is a 1,4 coupling between (Cα−Cβ) and (Cα−Cm). Of all of the bond types, the (Cα−N) couples strongly most promiscuously to other stretches, participating in 8 of the 14 large, long range, stretch−stretch interactions. In general, the (Cα−N) bonds couple fairly strongly to one another: the force constants for six of the seven possible unique, long range interactions have magnitudes greater than 8.5 kcal/(mol Å^2). In addition, (Cα−Cm)−(Cα−Cm) coupling can be quite strong. The 1,6 and 1,9 interactions have force constants of 19.9 and 25.8 kcal/(mol

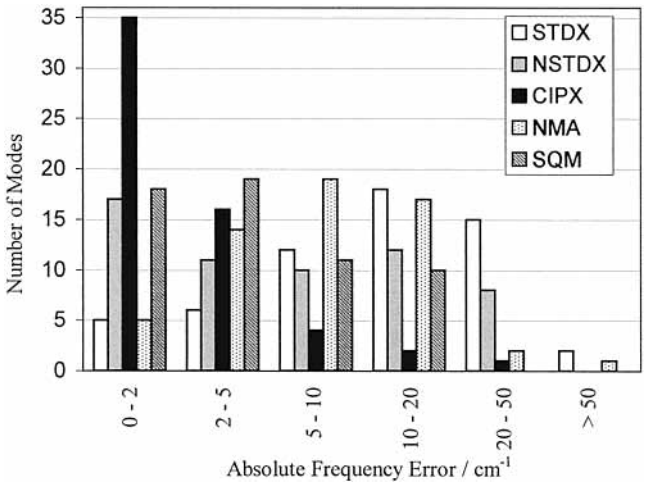

Figure 5. Performance of NMA, SQM, and HBFF-SVD force fields. The number of modes with absolute errors of 0−2, 2−5, 5−10, 10−20, 20−50, and >50 cm^{-1} relative to experimental measurements are reported for NMA, SQM, and the HBFF-SVD force fields STDX, NSTDX, and CIPX. The values for NMA and SQM are from ref 18.

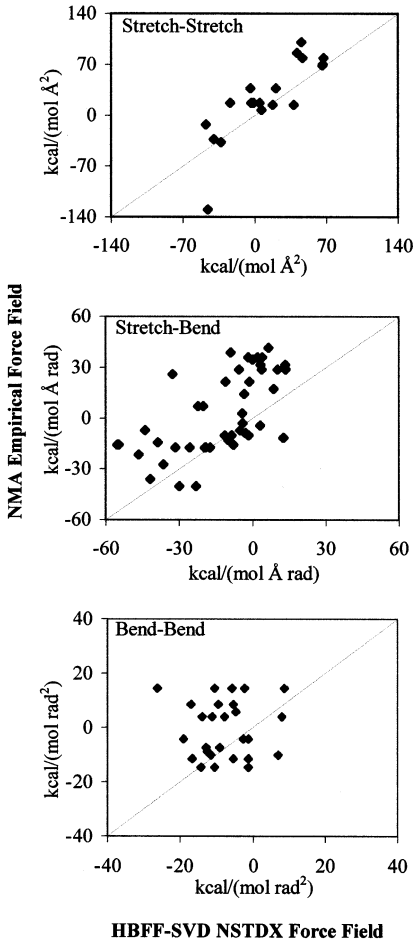

Figure 6. Comparison of NMA and HBFF-SVD NSTDX off-diagonal force constants. Stretch−stretch (kcal mol^{-1} $Å^{-2}$), stretch−bend (kcal mol^{-1} $Å^{-1}$ rad^{-1}), and bend−bend (kcal mol^{-1} rad^{-2}) force constants from the NMA empirical force field and the HBFF-SVD NSTDX force field are compared. The lines indicate the hypothetical situation in which the terms from the two force fields would be equal. The values for the NMA force constants from ref 18.

$Å^2$), respectively. Interestingly, the 1,8-(C_α−C_m)−(C_α−C_m) pairing suggested by Hu et al. [13] to be large, was found in the complete (CIPX) force field to be quite weak (0.7 kcal/(mol $Å^2$)). This will be addressed more fully in the next section.

The 1,9-(C_β−C_α−C_m)−(C_β−C_α−C_m) and 1,6-(C_β−C_α−N)−(C_α−C_m−C_α) interactions are the largest of the long range, bend−bend terms. Fewer of these types of terms are large for the trivial reason that the angle-bend force constants are smaller in magnitude than the bond stretch.

There are a surprisingly large number of significant, long range, stretch−bend terms. The largest is the intra-pyrrole (C_β−C_β)−(C_α−N−C_α) (33.2 kcal/(mol Å rad)) discussed above. In fact, though the (C_β−C_β) bond does not appear to couple strongly to other stretches about the macrocycle, it participates in half of the strongest (>15 kcal/(mol Å rad)) bend−stretch interactions. Neglecting the C_β−C_β stretch in long range interactions is thus unadvisable. These long range terms contribute significantly to the overall energy landscape. The terms listed in Tables 8 and 9 are all greater than 1% of the diagonal bond-stretch force constant mean, and more than 6% of the diagonal angle-bend force constant mean, which makes them comparable in size to many of the 1,3 interactions. All but one of these significant long range interactions have not been previously identified in NMA or SQM studies of NiP.

Though the remainder of the long range terms are smaller, they contribute in collective. It may be, though, that most of the 200+ smaller terms unnecessarily complicate the force field. It would be interesting to evaluate a force field between NSTDX and CIPX in complexity, using CIPX as a guide. For example, omitting the very weak (C_β−C_β)−(C_β−C_β) interactions should have an undetectable effect on force field quality. A subset of long range cross terms could be chosen using a cutoff value determined by evaluating CIPX. Reoptimization is necessary because of the cumulative effect of the large number of even very small terms. This approach is analogous to NMA, with the decided advantage that the selection of cross terms is much less subjective. The value of the CIPX fitting is that it identifies the "naturally" important long range cross terms.

TORX couples stretches and bends with torsions. These in- and out-of-plane interactions are more important for highly distorted porphyrins than for (nearly planar) NiP.[25] Nonetheless, the breakdown of the vibrational selection rules that allows several of the E_g modes to become slightly IR-active,[18] and the flat nature of the potential energy surface from 0° to ∼30° along the rufling coordinate,[66] indicate that out-of-plane motion may have some significance in NiP. The discussion of the force field geometry above suggests that the Fourier expansion used for the out-of-plane diagonal and cross terms may not be the most appropriate form to use. Unger et al. have proposed a very promising potential term ($V^{\pi\tau\tau}$) that works quite well for conjugated molecules, including porphyrins.[24,25] In future studies, clearly a better treatment of the out-of-plane motion must be explored, particularly for treatment of highly distorted porphyrins.

Comparison with NMA and SQM. The advantages and disadvantages of NMA, SQM, and the HBFF-SVD method have been discussed in the Introduction and will not be reiterated. In terms of complexity, the NMA force field falls somewhere between STDX and NSTDX. The SQM force field is, in principle, equivalent to CIPX. In this section, the force fields and their performances are compared. The NMA and SQM results discussed in this section are from Kozlowski et al.[18]

Examination of the rms errors shows that the ability of the higher complexity HBFF-SVD force fields to reproduce the experimental natural abundance frequencies was quite good (Table 4). NMA values are not available for the out-of-plane motions, but the in-plane vibrations were predicted by the NSTDX force field (rms error = 12.0 cm^{-1}) slightly better than

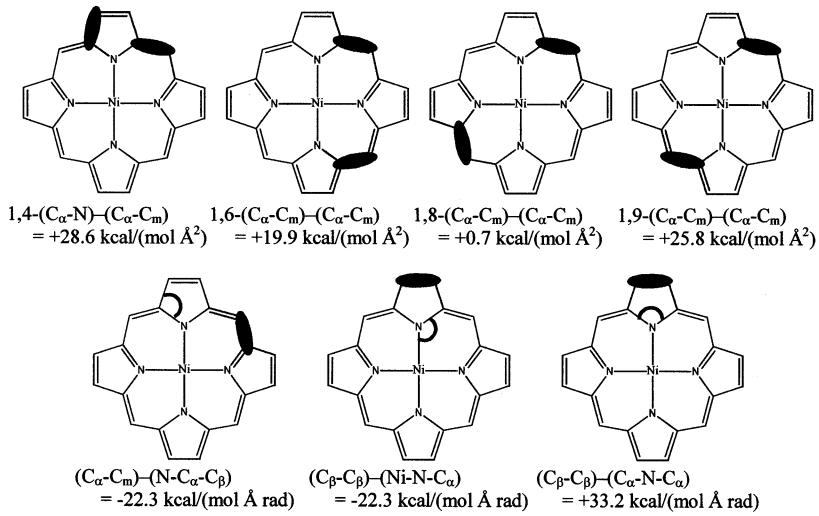

Figure 7. Selected Long range cross terms from the HBFF-SVD CIPX force field. The dark ovals and curves indicate bond stretches and angle bends, respectively, coupled for each term shown.

NMA (rms error = 12.8 cm^{-1}) and worse than SQM (rms error = 6.7 cm^{-1}). The CIPX force field is more accurate than both NMA and SQM, with a rms error for the in-plane motions of only 4.8 cm^{-1}.

Comparisons can also be made in the error distribution of the in-plane frequencies (Figure 5). CIPX is excellent, with 35 of the 58 available experimental frequencies within 2 cm^{-1} of their measured values. NSTDX and SQM are comparable, with 17 and 18 modes $\leq$2 cm^{-1} absolute error, respectively. In the 10−20 cm^{-1} range, CIPX again performs better with only 2 modes, whereas NSTDX and SQM have 12 and 10 modes with this larger absolute error, respectively. Here, also, it can be seen that NSTDX and CIPX are significantly superior to NMA, whereas STDX is slightly worse. On the other hand, SQM is between NSTDX and CIPX in accuracy.

The out-of-plane degrees of freedom were fit considerably more poorly by all HBFF-SVD force fields than by SQM. NMA out-of-plane results for NiP are not available for comparison. The rms error for DIAG, STDX, NSTDX, and CIPX was about 21 cm^{-1} and was lowered to 9.3 cm^{-1} in the TORX force field. SQM performed much better, with an out-of-plane rms error of only 5.1 cm^{-1}. This result is anticipated because the HBFF-SVD out-of-plane force fields contain no cross terms coupling out-of-plane degrees of freedom. Inclusion of these sorts of torsion−torsion, inversion−torsion, etc. terms would improve the fit. The poor fit of the out-of-plane coordinates led to poorer overall performance of the HBFF-SVD force fields relative to SQM.

Another measure of the quality of the force field is its ability to accurately reproduce isotopic vibrational shifts. It is a bit difficult to compare HBFF-SVD with SQM and NMA here, because both of the latter approaches utilized the experimental isotope shifts as parameters in optimizing the resultant force fields. The HBFF-SVD force fields did not include the isotope shift information in the optimization procedure. Despite this disadvantage, all of the HBFF-SVD force fields (DIAG was not evaluated) performed significantly better than NMA, and only slightly worse than SQM (Table 5). Results for the out-of-plane modes are not available for the NMA force field; however isotope shifts for the in-plane vibrations were calculated by NMA with rms errors of 13.7 cm^{-1} (NiP-d_4), 89.2 cm^{-1} (NiP-d_8), and 67.8 cm^{-1} (NiP-d_{12}). These results, particularly those of and NiP-d_8 and -d_{12}, are considerably poorer than even the STDX force field results and are nearly an order of magnitude less accurate than NSTDX and CIPX.

Both in-plane and out-of-plane results are available for the SQM force field. The NiP-d_4 isotope shifts were calculated with 4.2 cm^{-1}, the NiP-d_8 with 4.8 cm^{-1} and the NiP-d_{12} with 5.8 cm^{-1} of total rms accuracy. These represent improvements over NSTDX of only 1.8, 5.4, and 2.2 cm^{-1}, respectively, and over CIPX of 1.2, 3.5, and 1.3 cm^{-1}, respectively, in total rms accuracy. Given that the SQM force field was fit to the isotope shifts and the HBFF-SVD force fields were not, this result speaks very well for the HBFF-SVD method.

Qualitative comparison of the force constants, diagonal and off-diagonal, in the NMA and HBFF-SVD force fields is instructive (Tables 7−9, Figure 6). It is more difficult to discuss the SQM force field, as the natural internal coordinate system is quite different from the highly redundant one used in HBFF-SVD, and most of the SQM force constants have not been reported. We therefore focus on comparing the NSTDX and CIPX force fields with NMA, and only comment on SQM results where possible. Because the highly redundant coordinates employed in the NMA and HBFF-SVD studies differ, only qualitative comparisons can be done.

The strength ordering of the diagonal bond-stretch force constants is very similar for NMA and HBFF-SVD. Only the Ni−N force constant significantly differs: ~11% smaller for NSTDX and CIPX than for NMA. The angle-bend diagonal force constants also are similar. The main difference here is for (C_α−C_m−C_α). In NMA, this term is larger and approximately equal to that for (C_α−C_β−C_β). The NSTDX and CIPX force fields find that the (C_α−C_m−C_α) force constant is significantly smaller than that of (C_α−C_β−C_β) and that of NMA. These differences in diagonal force constants can be ascribed to the presence of additional, necessary cross terms involving the C_α−C_m bonds and angles, in particular, in the NSTDX and CIPX force fields.

The 1,2 and 1,3 interaction force constants available in both NMA and the NSTDX force field have been compared in Figure 6. The stretch−stretch terms show the highest degree of correlation, and the bend−bend terms the lowest. For all three types of interactions, the NMA terms are skewed to somewhat higher values. Again, this probably results from the increased number of important cross terms included in the NSTDX and CIPX force fields relative to NMA. That is, each cross term in the NMA force field must do more correcting than it should.

The long range cross terms in CIPX are very interesting. Hu et al.[13] discuss the importance of long range (C_α−C_m) interactions and find that including 1,8- and 1,9-(C_α−C_m)−(C_α−C_m)

stretch−stretch cross terms of −24.4 and +24.4 kcal/(mol Å^2), respectively, is important for obtaining high-quality results, particularly for modes involving $C_\alpha-C_m$ motion (e.g., ν_{10} and ν_{38}). The CIPX force field also found that long range ($C_\alpha-C_m$)−($C_\alpha-C_m$) coupling is important. However, the nature of the coupling is fundamentally different from that proposed previously. Hu et al.[13] make a resonance argument that the 1,8 interaction should be negative, the 1,9 interaction positive, and the 1,4 and 1,5 interactions zero. They do not mention the 1,6 interaction. Using HBFF-SVD, however, we found that the 1,8 interaction was very small (0.7 kcal/(mol Å^2)) and both the 1,6 and 1,9 interactions were large and positive, with values of 19.9 and 25.8 kcal/(mol Å^2), respectively. These interactions are depicted in Figure 7. The other long range ($C_\alpha-C_m$)−($C_\alpha-C_m$) interactions were found to be less than 5 kcal/(mol Å^2). With SQM, Kozlowski et al. also found a significant positive 1,6 interaction.[18] In both the SQM and CIPX force fields, the largest interaction is the 1,9, but whereas the CIPX 1,8 term is nearly zero, it is similar to the 1,6 term in magnitude in SQM, and positive, in contrast to NMA.

This disagreement points to a couple of difficulties in using resonance arguments for NiP. The use of resonance structures to evaluate cross terms is not straightforward in this system. First, there are often several equivalent binary pairs of couplings of a given type. For example, there are four equivalent 1,8-($C_\alpha-C_m$)−($C_\alpha-C_m$) couplings, and eight equivalent 1,5 interactions. Evaluation of only one member of each class can be misleading. Had Hu et al. chosen the 2′,9- and 2′,8-($C_\alpha-C_m$)−($C_\alpha-C_m$) interactions (see Figure 6, Hu et al.[13]) rather than the entirely equivalent 1,8 and 1,9 pairs, they would have predicted the opposite signs for their cross terms.

A larger problem with using simple resonance arguments for NiP is that it is not a "simple" conjugated system. Multiple resonance structures produce branching behavior at the C_α's. In addition, the pyrroles themselves are conjugated. Thus the classic picture of alternating algebraic signs for stretch−stretch cross terms along the conjugation path does not hold for the metalloporphyrin macrocycle, though the strengths do alternate, as shown in Figure 3 and in Figure 4 of Kozlowski et al.[18] This makes it difficult to predict a priori the magnitude and sign of a given cross term. Here, allowing all of the ($C_\alpha-C_m$)−($C_\alpha-C_m$) interactions to fit to their "natural" values, we found two large, positive terms and no significant negative coupling.

Several other considerably important long range cross terms have not previously been identified. One heretofore unrecognized, particularly significant term is the intrapyrrole coupling between the $C_\beta-C_\beta$ bond and the $C_\alpha-N-C_\alpha$ angle (33 kcal/(mol Å rad)). Others are listed in Tables 8 and 9. These terms are omitted in the treatment NMA of NiP and were not identified by SQM. Kozlowski et al. reported that "no off-diagonal elements were neglected in the empirical (NMA) FF which have substantial ab initio values."[18] The conflict with SQM may be partly in the definition of "substantial", as examination of Figure 4 of ref 18 shows a few terms of significant magnitude. Also, SQM treatment of H_2-porphine provided several significant, long range interactions.[16] In any case, it is clear from the very high quality of the CIPX force field in reproducing the in-plane vibrational frequencies of both the natural abundance and isotopically substituted NiP that these long range cross terms are necessary.

The hybrid force field discussed above, in which CIPX results are used to objectively separate long range terms into "naturally important" and "unimportant" subsets, is an excellent alternative to the NMA, SQM, and HBFF-SVD CIPX treatments. It would reduce the complexity of the redundant force field without sacrificing objectivity, accuracy, or utility of form.

IV. Summary

In summary, this manuscript reports a systematic exploration of the importance of cross terms, particularly long range, in the force field of an important "standard" metalloporphyrin, NiP. The results of this HBFF-SVD treatment are compared to previous NMA and SQM studies. Several force fields of varying complexity were generated using the experimental crystal structure, a B3LYP/6-31G(d,p) Hessian matrix, and experimental vibrational frequencies. The simplest, diagonal-only (DIAG) force field was inadequate for reproducing experimental frequencies. The inclusion of 1,2 and 1,3 cross terms (NSTDX) led to a force field significantly superior to that of NMA. The longer range, in-plane cross terms present in CIPX improved the performance for the in-plane modes, generating a force field slightly superior to that of SQM for the in-plane degrees of freedom in the natural abundance spectrum. For the isotopically shifted spectra, all of the HBFF-SVD force fields represented a significant improvement over NMA but performed slightly more poorly than SQM. This result is particularly promising, as the isotopic shifts were not used to optimize the HBFF-SVD force fields but were used in the NMA and SQM optimizations. Coupling of in-plane and out-of-plane motions improved the out-of-plane motion, particularly the low frequency doming, but did not affect the in-plane accuracy significantly. Finally, the CIPX force field pointed out the difficulty of using resonance arguments in this system for intuiting which long range cross terms should be significant in this complicated system. Several previously unidentified, important, long range cross terms were discovered and explored. These interactions are crucial in accurately reproducing the vibrational behavior of the porphyrin, and in understanding the fundamental nature of the structure-spectrum relationship.

Acknowledgment. M.C.S. acknowledges the support of the Department of Energy Distinguished Postdoctoral Research Program and the National Institutes of Health (GM056816). M.C.S. also thanks Professor W. A. Goddard, III and Dr. S. Dasgupta for helpful conversations early in this study.

Supporting Information Available: Diagonal force constants (Table S1), 1,2 cross term force constants (Table S2), 1,3 cross term force constants (Table S3), and long range cross term force constants (Table S4). This material is available free of charge via the Internet at http://pubs.acs.org.

References and Notes

(1) *The Porphyrin Handbook*; Kadish, K. M., Smith, K. M., Guilard, R., Eds.; Academic Press: New York, 2000; Vol. 7.

(2) Spiro, T. G.; Czernuszewicz, R. S.; Li, X.-Y. *Coord. Chem. Rev.* **1990**, *100*, 541−571.

(3) Spiro, T. G.; Loehr, T. M. Resonance Raman Spectra of Heme Proteins and other Biological Systems. In *Advances in IR and Raman Spectroscopy*; 1975; Vol. 1, Chapter 3.

(4) *J. Porphyrins Phthalocyanines* **2001**, *5*, 187−364 (special volume).

(5) Ghosh, A. *Acc. Chem. Res.* **1998**, *31*, 189−198.

(6) Ghosh, A. Quantum Chemical Studies of Molecular Structures and Potential Energy Surfaces of Porphyrins and Hemes. In *Theoretical and Physical Characterization*; Kadish, K. M., Smith, K. M., Guilard, R., Eds.; The Porphyrin Handbook, Vol. 7; Academic Press: New York, 2000; pp 1−38.

(7) Abe, M.; Kitagawa, T.; Kyogoku, Y. *J. Chem. Phys.* **1978**, *69*, 4526.

(8) Abe, M. Normal Coordinate Analysis of Large Molecules of Biological Interest: Metalloporphyrins and Lumiflavin. In *Spectroscopy of Biological Systems*; Wiley: New York, 1986; pp 347−393.

(9) Kitagawa, T.; Abe, M.; Ogoshi, H. *J. Chem. Phys.* **1978**, *69*, 4516−4525.
(10) Li, X.-Y.; Czernuszewicz, R. S.; Kincaid, J. R.; Su, Y. O.; Spiro, T. G. *J. Phys. Chem.* **1990**, *94*, 31−47.
(11) Li, X.-Y.; Czernuszewicz, R. S.; Kincaid, J. R.; Stein, P.; Spiro, T. G. *J. Phys. Chem.* **1990**, *94*, 47−61.
(12) Li, X.-Y.; Czernuszewicz, R. S.; Kincaid, J. R.; Spiro, T. G. *J. Am. Chem. Soc.* **1989**, *111*, 7012−7023.
(13) Hu, S.; Mukherjee, A.; Piffat, C.; Mak, R. S. W.; Li, X.-Y.; Spiro, T. G. *Biospectroscopy* **1995**, *1*, 395−412.
(14) Jarzecki, A. A.; Kozlowski, P. M.; Pulay, P.; Ye, B. h.; Li, X.-Y. *Spectrochim. Acta A* **1997**, *53*, 1195−1209.
(15) Kozlowski, P. M.; Zgierski, M. Z.; Pulay, P. *Chem. Phys. Lett.* **1995**, *247*, 379−385.
(16) Kozlowski, P. M.; Jarzecki, A. A.; Pulay, P. *J. Phys. Chem.* **1996**, *100*, 7007−7013.
(17) Kozlowski, P. M.; Jarzecki, A. A.; Pulay, P.; Li, X.-Y.; Zgierski, M. Z. *J. Phys. Chem.* **1996**, *100*, 13985−13992.
(18) Kozlowski, P. M.; Rush, T. S., III; Jarzecki, A. A.; Zgierski, M. Z.; Chase, B.; Piffat, C.; Ye, B.-H.; Li, X.-Y.; Peter, P.; Spiro, T. G. *J. Phys. Chem. A* **1999**, *103*, 1357−1366.
(19) Shelnutt, J. A.; Song, X.-Z.; Ma, J.-G.; Jia, S.-L.; Jentzen, W.; Medforth, C. J. *Chem. Soc. Rev.* **1998**, *27*, 31−41.
(20) Fajer, J. *J. Porphyrins Phthalocyanines* **2000**, *4*, 382−385.
(21) Shelnutt, J. A. Molecular Simulations and Normal-Coordinate Structural Analysis of Porphyrins and Heme Proteins. In *Theoretical and Physical Characterization*; Kadish, K. M., Smith, K. M., Guilard, R., Eds.; The Porphyrin Handbook, Vol. 7; Academic Press: New York, 2000; pp 167−223.
(22) Wilson, E. B. J.; Decius, J. C.; Cross, P. C. *Molecular Vibrations. The Theory of Infrared and Raman Vibrational Spectra*; Dover Publications: New York, 1955.
(23) Rush, T. S.; Kozlowski, P. M.; Piffat, C. A.; Kumble, R.; Zgierski, M. Z.; Spiro, T. G. *J. Phys. Chem. B* **2000**, *104*, 5020−5034.
(24) Unger, E.; Lipski, R. J.; Dreybrot, W.; Schweizer-Stenner, R. *J. Raman Spectrosc.* **1999**, *30*, 3−28.
(25) Unger, E.; Beck, M.; Lipski, R. J.; Dreybrot, W.; Medforth, C. J.; Smith, K. M.; Schweizer-Stenner, R. *J. Phys. Chem. B* **1999**, *103*, 10022−10031.
(26) Hehre, W. J.; Radom, L.; Schleyer, P. V. R.; Pople, J. A. *Ab Initio Molecular Orbital Theory*; John Wiley & Sons: New York, 1986.
(27) Koch, W.; Holthausen, M. C. *A Chemist's Guide to Density Functional Theory*; Wiley-VCH Verlag: Weinheim, 2000.
(28) Wong, M. W. *Chem. Phys. Lett.* **1996**, *256*, 391−399.
(29) Pople, J. A.; Schlegel, H. B.; Krishnan, R.; DeFrees, D.; Binkley, J. S.; Frisch, M. J.; Whiteside, R. F.; Hout, R. F.; Hehre, W. J. *Int. J. Quantum Chem.* **1981**, Suppl. 15, 269−278.
(30) *Spectrochim. Acta Part A* **1997**, *53*, 1039−1363 (special volume).
(31) Pulay, P.; Fogarasi, G.; Pongor, G.; Boggs, J. E.; Vargha, A. *J. Am. Chem. Soc.* **1983**, *105*, 7037−7047.
(32) Fogarasi, G.; Zhou, X.; Patterson, W. T.; Pulay, P. *J. Am. Chem. Soc.* **1992**, *114*, 8191−8201.
(33) Rauhut, G.; Pulay, P. *J. Phys. Chem.* **1995**, *99*, 3093−3100.
(34) Baker, J.; Jarzecki, A. A.; Pulay, P. *J. Phys. Chem. A* **1998**, *102*, 1412−1424.
(35) Dasgupta, S.; Goddard, W. A. *J. Chem. Phys.* **1989**, *90*, 7207−7215.
(36) Dasgupta, S.; Yamasaki, T.; Goddard, W. A. *J. Chem. Phys.* **1996**, *104*, 2898−2920.
(37) Dasgupta, S.; Brameld, K. A.; Fan, C.-F.; Goddard, W. A. *Spectrochim. Acta Part A* **1997**, *53*, 1347−1363.
(38) Demiralp, E.; Dasgupta, S.; Goddard, W. A. *J. Phys. Chem. A* **1997**, *101*, 1975−1981.
(39) Demiralp, E.; Goddard, W. A. *J. Phys. Chem. A* **1998**, *102*, 2466−2471.
(40) Jiang, S.; Dasgupta, S.; Blanco, M.; Frazier, R.; Yamaguchi, E. S.; Tang, Y.; Goddard, W. A. *J. Phys. Chem.* **1996**, *100*, 15760−15769.
(41) Karasawa, N.; Dasgupta, S.; Goddard, W. A. *J. Phys. Chem.* **1991**, *95*, 2260−2272.
(42) Musgrave, C. B.; Dasgupta, S.; Goddard, W. A. *J. Phys. Chem.* **1995**, *99*, 13321−13333.
(43) Wendel, J. A.; Goddard, W. A. *J. Chem. Phys.* **1992**, *97*, 5048−5062.
(44) Jentzen, W.; Turowska-Tyrk, I.; Schedit, W. R.; Shelnutt, H. *Inorg. Chem.* **1996**, *35*, 3559−3567.
(45) Frisch, M. J.; Trucks, G. W.; Schlegel, H. B.; Scuseria, G. E.; Robb, M. A.; Cheeseman, J. R.; Zakrzewski, V. G.; Montgomery, J. A.; Stratmann, R. E.; Burant, J. C.; Dapprich, S.; Millam, J. M.; Daniels, A. D.; Kudin, K. N.; Strain, M. C.; Farkas, O.; Tomasi, J.; Barone, V.; Cossi, M.; Cammi, R.; Mennucci, B.; Pomelli, C.; Adamo, C.; Clifford, S.; Ochterski, J.; Petersson, G. A.; Ayala, P. Y.; Cui, Q.; Morokuma, K.; Malick, D. K.; Rabuck, A. D.; Raghavachari, K.; Foresman, J. B.; Cioslowski, J.; Ortiz, J. V.; Stefanov, B. B.; Liu, G.; Liashenko, A.; Piskorz, P.; Komaromi, I.; Gomperts, R.; Martin, R. L.; Fox, D. J.; Keith, T.; Al-Laham, M. A.; Peng, C. Y.; Nanayakkara, A.; Gonzalez, C.; Challacombe, M.; Gill, P. M. W.; Johnson, B. G.; Chen, W.; Wong, M. W.; Andres, J. L.; Head-Gordon, M.; Replogle, E. S.; Pople, J. A. *Gaussian 98*, Revision A.9; Gaussian, Inc.: Pittsburgh, PA, 1998.
(46) Becke, A. D. *Phys. Rev. A* **1988**, *39*, 3098.
(47) Lee, C.; Yang, W.; Parr, R. G. *Phys. Rev. B* **1988**, *37*, 785.
(48) Becke, A. D. *J. Chem. Phys.* **1993**, *98*, 5648−5652.
(49) Petersson, G. A.; Al-Laham, M. A. *J. Chem. Phys.* **1991**, *94*, 6081.
(50) Almlof, J.; Fishcer, T. H.; Gassman, P. G.; Ghosh, A.; Haser, M. *J. Phys. Chem.* **1993**, *97*, 10964−10970.
(51) Karpfen, A.; Choi, C. H.; Kertesz, M. *J. Phys. Chem. A* **1997**, *101*, 7426−7433.
(52) Hoard, J. L. *Science* **1971**, *174*, 1295.
(53) Shelnutt, J. A.; Medforth, C. J.; Berber, M. D.; Barkigia, K. M.; Smith, K. M. *J. Am. Chem. Soc.* **1991**, *113*, 4077−4087.
(54) Press: W.; Teukolsky, S. A.; Vetterling, W. T.; Flannery, B. P. *Numerical Recipes in Fortran*; Cambridge University Press: Cambridge, U.K., 1992.
(55) Weiner, P. K.; Kollman, P. A. *J. Comput. Chem.* **1981**, *2*, 287−303.
(56) Weiner, S. J.; Kollman, P. A.; Case, D. A.; Singh, U. C.; Ghio, C.; Alagona, G.; Profeta, S. J.; Weiner, P. K. *J. Am. Chem. Soc.* **1984**, *106*, 765−784.
(57) Weiner, S. J.; Kollman, P. A.; Nguyen, D. T.; Case, D. A. *J. Comput. Chem.* **1986**, *7*, 230−252.
(58) Pearlman, D. A.; Case, D. A.; Caldwell, J. C.; Seibel, G. L.; Singh, U. C.; Weiner, P.; Kollman, P. A. *AMBER*, 4.0 ed.; University of California, San Francisco: San Francisco, 1991.
(59) Cornell, W. D.; Cieplak, P.; Bayly, C. I.; Gould, I. R.; Merz, K. M., Jr.; Ferguson, D. M.; Spellmeyer, D. C.; Fox, T.; Caldwell, J. W.; Kollman, P. A. *J. Am. Chem. Soc.* **1995**, *117*, 5179.
(60) Young, D. *Computational Chemistry: A Pratical Guide for Applying Techniques to Real World Problems*; John Wiley & Sons: New York, 2001.
(61) Kaminski, G.; Duffey, E. M.; Matsui, T.; Jorgensen, W. L. *J. Phys. Chem.* **1994**, *98*, 13077−13082.
(62) Jorgensen, W. L.; Tirado-Rives, J. *J. Am. Chem. Soc.* **1988**, *110*, 1657−1666.
(63) Jorgensen, W. L.; Maxwell, D. S.; Tirado-Rives, J. *J. Am. Chem. Soc.* **1996**, *118*, 11225−11236.
(64) Damm, W.; Forntera, A.; Tirado-Rives, J.; Jorgensen, W. L. *J. Comput. Chem.* **1997**, *18*, 1955−1970.
(65) Dauber-Osguthorpe, P.; Roberts, V. A.; Osguthorpe, D. J.; Wolff, J.; Genest, M.; Hagler, A. T. *Proteins: Structure, Function and Genetics* **1988**, *4*, 31−47.
(66) Tsai, H.-H.; Simpson, M. C. *J. Phys. Chem. A*, to be submitted.